Chaotic motions in the restricted four body problem via Devaney's saddle-focus homoclinic tangle theorem

Shane Kepley * [1] and J.D. Mireles James †[2]

[1]Rutgers University, Department of Mathematics
[2]Florida Atlantic University, Department of Mathematical Sciences

March 6, 2018

Abstract

We prove the existence of chaotic motions in an equilateral planar circular restricted four body problem (CRFBP), establishing that the system is not integrable. The proof works by verifying the hypotheses of a topological forcing theorem for Hamiltonian vector fields on $\mathbb{R}^4$ which hypothesizes the existence of a transverse homoclinic orbit in the energy manifold of a saddle focus equilibrium. We develop mathematically rigorous computer assisted arguments for verifying these hypotheses, and provide an implementation for CRFBP. Due to the Hamiltonian structure, this also establishes the existence of a "blue sky catastrophe", and hence an analytic family of periodic orbits of arbitrarily long period at nearby energy levels.

Our method works far from any perturbative regime and requires no mass symmetry. Additionally, the method is constructive and yields additional byproducts such as the locations of transverse connecting orbits, quantitative information about the invariant manifolds, and bounds on transport times.

1 Introduction

The study of gravitational N-body problems and the development of the qualitative theory of dynamical systems have progressed hand in hand for more than a century. Because N-body interactions introduce strong nonlinearities it is not possible, except in certain symmetrical or perturbative cases, to answer dynamical questions about specific systems without resorting to numerical calculations. Objects like relative equilibria, periodic orbits, connecting orbits, and binary collisions were studied numerically long before the advent of digital computing. The 1897 paper of George Darwin [1], the work of the group of Forest Ray Moulton at the University of Chicago from 1900 until the 1930's [2], and the work of the group of Elis Strömgren at the Copenhagen Observatory from 1907 until 1940 [3], provide early yet surprisingly modern examples of numerical treatment of N-body

*S.K. partially supported by NSF grant DMS-1700154 and by the Alfred P. Sloan Foundation grant G-2016-7320. Email: skepley@my.fau.edu

†J.D.M.J partially supported by NSF grant DMS-1700154 and by the Alfred P. Sloan Foundation grant G-2016-7320. Email: jmirelesjames@fau.edu

dynamics. A thorough and scholarly review of early twentieth century dynamical astronomy, focusing on numerical results, is found in Chapters $9.11 - 9.12$ of the classic book of Szebehely [4]. In particular, Chapter 9.12 includes a complete list of over 60 references to relevant publications by the Copenhagen group from 1913 to 1939.

The work of the Copenhagen group is especially relevant to the present discussion. For more than 30 years they studied the behavior of the planar circular restricted three body problem (CRTBP), and their research led Strömgren to conjecture that some one parameter families of periodic orbits terminate at "asymptotic-periodic orbits" of infinite period. These infinitely long cycles would be called heteroclinic or homoclinic orbits in modern termenology. This became known as the Strömgren conjecture, and is the topic of many subsequent investigations including the 1960 Ph.D. thesis of Shearing [5], the papers of Bartlett in 1964 and 65 [6, 7], the 1965 paper of Henon [8], the 1967 paper of Danby [9], and in the 1967 papers of Szebehely, Narcoz, and Flandern [10, 11] to name a few. Each of these papers exploited the newly available power of the digital computer and taken together, they provide compelling numerical evidence supporting Strömgren's insights. To frame the discussion in modern language we make the following definition.

Definition 1 (Strömgren hypothesis)**.** Let $U \subset \mathbb{R}^4$ be an open set and $f\colon U \to \mathbb{R}^4$ be a real analytic Hamiltonian vector field with the conserved quantity $H\colon U \to \mathbb{R}$. Suppose that $\mathbf{x}_0 \in U$ is an equilibrium point whose eigenvalues are $\pm\alpha \pm i\beta$ with $\alpha, \beta > 0$. We say that f satisfies the *Strömgren hypothesis* if there exists a transverse homoclinic orbit $\gamma\colon \mathbb{R} \to U$ for $\mathbf{x}_0$.

We refer to $\mathbf{x}_0$ as a saddle-focus, and to H as the energy of the system. The notion of transversality in the definition is relative to the energy manifold of the equilibrium, as generic vector fields do not admit transverse homoclinics. However a pair of two dimensional (stable/unstable) manifolds for the four dimensional phase space of a two freedom Hamiltonian system may intersect transversally in the three dimensional energy manifold of the equilibrium. Indeed the resulting homoclinic orbit is structurally stable in the category of Hamiltonian perturbations.

The conjecture is now rephrased as follows: Does the Strömgren hypothesis imply the existence of a family of periodic orbits limiting to the homoclinic γ? In 1973 Henrard addressed the problem from an analytical perspective, with the following result appearing as Theorem I in [12].

Theorem 1.1 (Blue Sky Catastrophe)**.** *Assume that $f\colon U \to \mathbb{R}^4$ satisfies the Strömgren hypothesis of Definition 1. Then, near γ there exists a one parameter family (or "tube") of periodic orbits accumulating to γ. This tube depends analytically on the energy with the period of the orbits going to infinity, and the stability of this family changes infinitely often as $H \to H(\mathbf{x}_0)$.*

The name blue sky catastrophe was attached to this phenomenon by Abraham in [13], and the interested reader might consult also the works of Devaney, Lerman, or L.P. Shilnikov, A.L. Shilnikov, and Turaev in, [14, 15, 16] respectively.

The occurrence of infinitely many stability changes as $H \to H(\mathbf{x}_0)$ suggests a period doubling bifurcation, and perhaps the existence of rich dynamics near the homoclinic. Indeed, numerical evidence for the existence of Feigenbaum cascades in the CRTBP resulting from a blue sky catastrophe appears in the works of Pinotsis and Sicardy [17, 18]. Complicated dynamics near γ are considered from an analytical perspective as early as the 1976 paper of Devaney [19], where the following topological forcing theorem appears as Theorem A.

Theorem 1.2 (Hamiltonian saddle-focus homoclinic tangle theorem)**.** *If $f\colon U \to \mathbb{R}^4$ satisfies the Strömgren hypothesis, and if Σ is any local transverse section to γ, then for any positive integer N*

there is a compact, invariant, hyperbolic set $\Lambda_N \subset \Sigma$ on which the Poincaré map is topologically conjugate to the Bernoulli shift on N symbols.

The theorem is an adaptation of the classic homoclinic bifurcation of Shilnikov [20, 21], to the Hamiltonian setting. See also the works of Lerman [15, 22]. The theorem has much in common with Smale's homoclinic tangle theorem for diffeomorphisms [23]. Note however that the Devaney theorem implies infinite topological entropy in the energy level of the saddle-focus, whereas the classic theorem of Smale provides only a semi-conjugacy to the full shift on two symbols.

The goal of the present work is to develop a practical method for verifying the Strömgren hypothesis of Definition 1 in applications. Our work exploits the validated numerical tools for studying stable/unstable manifolds developed in [24, 25]. The method is applied to the specific example of a circular restricted four body problem (CRFBP) which we review in Section 1.1. The main result of the paper is the following theorem.

Theorem 1.3 (Existence of a CRFBP satisfying the Strömgren conjecture)**.** *The planar circular restricted four body problem with mass parameters $m_1 = 0.5$, $m_2 = 0.3$, and $m_3 = 0.2$ satisfies the Strömgren hypothesis of Definition 1.*

We then obtain the conclusions of Theorems 1.1 and 1.2 as corollaries.

The proof of the theorem is both constructive and non-perturbative, and it makes substantial use of the digital computer. While the results of Theorem 1.3 establish the Strömgren hypothesis only for a single set of parameters, our method does not depend on these parameter choices and it works in principle for any values of m_1, m_2, m_3, as well as other two freedom Hamiltonian systems admitting saddle-foci. Its worth mentioning two novelties of our approach before describing the method in detail.

- **Automatic transversality:** the computer assisted proof of Theorem 1.3 exploits Theorem 2.1, which is a result of Newton-Kantorovich type. An attractive feature of the Newton-like argument is that, whenever the hypotheses are verified, we automatically obtain non-degeneracy of the solution (in the sense that a certain Jacobian matrix is invertible). In Section 1.2 we exploit this by proving that the transversality condition in Strömgren's hypothesis is obtained from this non-degeneracy (almost) for free (we only have to check that the gradient of the energy at the homoclinic point is not zero). Earlier transversality results of this kind appear in [26, 27], however these previous results do not apply in an energy section.

- **Rigorous lower bounds on transfer times:** the argument of the present work exploits some validated numerical methods for growing atlases for stable/unstable manifolds which were recently developed by the authors in [25]. Because of the way we systematically grow the manifold atlas, we are also able to rule out connecting orbits. The ability to rule out orbits leads to lower bounds on transport times. This aspect of our approach is discussed further in Section 5.4.

Remark 1 (Rigorous results in the CRFBP and computer assisted proof). Mathematically rigorous results about the dynamics of the CRFBP are notoriously hard to come by. A case in point is the question of the number, location, and stability of the equilibria (also called the *libration points*). The 1977 paper of Simó provides a detailed numerical study of this question, and the results indicate that there are $8, 9$ or 10 equilibria depending on the ratios of the masses. This question has been resolved by Leandro and Barros in the papers [28, 29, 30], which provide complete mathematical

proof that the situation is just as described by Simó. From our point of view, it is important to stress that the proof makes substantial use of the digital computer.

Since even elementary questions about the zeros of the vector field cannot be settled without computer assistance, it is not surprising that global questions like those considered in the present work should employ the computer as well. Indeed, there is a rich tradition of computer assisted proof in the celestial mechanics literature, and the interested reader will find many additional results and references in the works of [31, 32, 33, 34, 35, 36, 37, 38, 39, 40, 41, 42, 43, 44, 45].

Finally we mention that our work is closely related to the 2013 study by Burgos-García and Delgado, wherein they consider the blue sky catastrophe near a Hamiltonian Hopf bifurcation in the CRFBP [46]. The authors focus on the case of two masses equal, performing a careful numerical analysis which combines Melnikov and normal form theory. An interesting future project would be to combine the validated numerical methods used in the present work with their approach to obtain a computer assisted proof of the blue sky catastrophe near the Hamiltonian Hopf bifurcation.

1.1 Review of the CRFBP

In this section, we introduce the mathematical formulation of the CRFBP. Consider three particles with masses $0 < m_3 \leq m_2 \leq m_1 < 1$, normalized so that

$$m_1 + m_2 + m_3 = 1,$$

arranged in a central configuration of Lagrange so that the masses are at the vertices of an equilateral triangle rotating with constant angular velocity. After changing to a co-rotating coordinate frame, we are interested in the dynamics of a fourth massless particle, p, with coordinates (x, y) moving in the gravitational field of the primaries. The situation is illustrated in Figure 1.

We refer to the three massive particles as the primary masses or simply as the *primaries*, and let (x_1, y_1), (x_2, y_2), and (x_3, y_3) denote their locations. Explicit formulas for these locations as a function of the mass parameters are recorded in Appendix C. Define the potential function

$$\Omega(x, y) := \frac{1}{2}(x^2 + y^2) + \frac{m_1}{r_1(x, y)} + \frac{m_2}{r_2(x, y)} + \frac{m_3}{r_3(x, y)}, \tag{1}$$

where

$$r_j(x, y) := \sqrt{(x - x_j)^2 + (y - y_j)^2}, \qquad j = 1, 2, 3. \tag{2}$$

Let $\mathbf{x} = (x, \dot{x}, y, \dot{y}) \in \mathbb{R}^4$ denote the state of the system. The equations of motion in the rotating frame are

$$\mathbf{x}' = f(\mathbf{x}),$$

where

$$f(x, \dot{x}, y, \dot{y}) := \begin{pmatrix} \dot{x} \\ 2\dot{y} + \Omega_x(x, y) \\ \dot{y} \\ -2\dot{x} + \Omega_y(x, y) \end{pmatrix}. \tag{3}$$

The system conserves the quantity

$$E(x, \dot{x}, y, \dot{y}) \quad = \tfrac{1}{2}\left(\dot{x}^2 + \dot{y}^2\right) - \Omega(x, y), \tag{4}$$

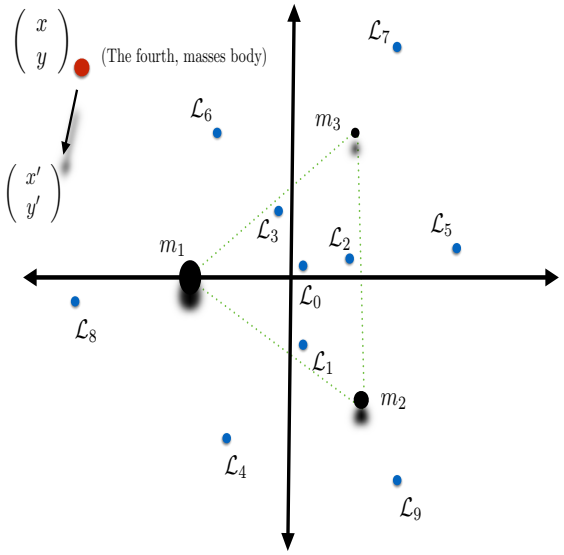

Figure 1: Configuration space for the CRFBP: The three primaries with masses m_1, m_2, and m_3 are arranged in the triangular relative equilibrium solution of Lagrange. We study the dynamics of a fourth massless particle like an asteroid or space craft in co-rotating coordinates. The problem admits 8, 9, or 10 (shown here) equilibrium solutions, 6 of which are always outside the triangle formed by the primary bodies.

which is called the *Jacobi integral*. We refer to E as "the energy" of the CRFBP, though strictly speaking the mechanical energy of the system is $-E$. Note that E is continuous (in fact real analytic) away from the primaries.

We conclude this section with a few general comments about the literature. The literature on libration points of the CRFBP was discussed already in Remark 1. Periodic solutions of the CRFBP are studied from theoretical and numerical viewpoints in [47, 48, 49]. The studies of [50, 51] consider also stable/unstable manifolds attached to periodic orbits. More global considerations such as connecting orbits and chaotic dynamics are studied from a numerical perspective in [52, 53, 54, 51]. Theoretical/pen and paper works on heteroclinic/homoclinic orbits and chaotic motions are found in the works of [46, 55, 56, 57], and use perturbative methods to establish the existence of complex dynamics. The work of [58] considers regularization of collisions with the primary bodies. A Hill's approximation is developed in [59].

1.2 The proof of Theorem 1.3

Let $U \subset \mathbb{R}^4$ be an open set with $f\colon U \to \mathbb{R}^4$ denoting the CRFBP vector field defined in Equation (3), and let $\Phi : U \times \mathbb{R} \to \mathbb{R}^4$ denote the flow generated by f. Assume $\mathbf{x}_0 \in \mathbb{R}^4$ is an equilibrium solution, and let $W^s(\mathbf{x}_0), W^u(\mathbf{x}_0)$ denote its stable and unstable manifolds respectively. Suppose that $\Gamma^s, \Gamma^u\colon [-1,1]^2 \subset \mathbb{R}^2 \to \mathbb{R}^4$ are smooth maps with

$$\Gamma^s([-1,1]^2) \subset W^u(\mathbf{x}_0) \qquad \text{and} \qquad \Gamma^u([-1,1]^2) \subset W^s(\mathbf{x}_0).$$

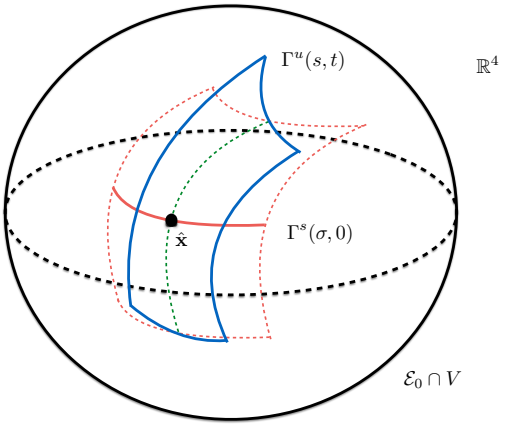

Figure 2: **The geometry of a transverse homoclinic**: $\mathcal{E}_0$ is the three dimensional energy section of the equilibrium $\mathbf{x}_0$ (not pictured) and U is a ball in $\mathbb{R}^4$ then the figure illustrates a transverse intersection of the stable and unstable manifolds at $\hat{\mathbf{x}} \in U \cap \mathcal{E}_0$. The parameterizations $\Gamma^{s,u}\colon [-1,1]^2 \to \mathbb{R}^4$ are charts for some neighborhoods of the stable and unstable manifolds $W^{s,u}(\mathbf{x}_0)$. These are represented respectively by the red and blue surface elements. By restricting Γ^s to its zero section – shown as the solid red curve – we isolate $\hat{\mathbf{x}}$. The desired homoclinic is the orbit through $\hat{\mathbf{x}}$ pictured as the dotted green line in the figure. The orbit lies in the transverse intersection of the stable/unstable manifolds, though the transversality is only relative to the energy section.

Components of the charts are denoted by $\Gamma^{s,u}_j$, for $j = 1,2,3,4$. Assume that $\Gamma^{s,u}$ are *well aligned* with the flow, in the sense that

$$\Phi(\Gamma^{s,u}(s,t_1), t_2/\tau_{s,u}) = \Gamma^{s,u}(s, t_1 + t_2), \tag{5}$$

for all t_1, t_2 so that $t_1 + t_2 \in [-1,1]$. Here $\tau_{s,u} > 0$ are reparameterizations of time associated with the stable/unstable charts. We begin by obtaining sufficient conditions for the situation depicted in Figure 2.

Lemma 1.4. *Define* $G\colon [-1,1]^3 \to \mathbb{R}^3$ *by*

$$G(s,t,\sigma) := \begin{pmatrix} \Gamma^u_1(s,t) - \Gamma^s_1(\sigma,0) \\ \Gamma^u_2(s,t) - \Gamma^s_2(\sigma,0) \\ \Gamma^u_3(s,t) - \Gamma^s_3(\sigma,0) \end{pmatrix},$$

and suppose $(\hat{s},\hat{t},\hat{\sigma}) \in [-1,1]^3$ *satisfies* $G(\hat{s},\hat{t},\hat{\sigma}) = 0$. *If* $\Gamma^u_4(\hat{s},\hat{t})$ *and* $\Gamma^s_4(\hat{\sigma},0)$ *have the same sign, then* $\hat{\mathbf{x}} := \Gamma^u(\hat{s},\hat{t})$ *is homoclinic to* $\mathbf{x}_0$.

Proof. Note that

$$\Gamma^s(s,t) = \Gamma^u(\sigma,\tau),$$

implies

$$\hat{\mathbf{x}} = \Gamma^s(s,t) \in W^s(\mathbf{x}_0) \cap W^u(\mathbf{x}_0),$$

and hence $\hat{\mathbf{x}}$ is homoclinic to $\mathbf{x}_0$. Restricting to the $\tau = 0$ section for Γ^u isolates an intersection point. Since $G(\hat{s}, \hat{t}, \hat{\sigma}) = 0$, it follows that $\Gamma^u(\hat{s}, \hat{t})$ and $\Gamma^s(\hat{\sigma}, 0)$ already agree in their first three components, and we consider the fourth.

Define the numbers

$$x^u = \Gamma_1^u(\hat{s}, \hat{t}), \qquad \dot{x}^u = \Gamma_2^u(\hat{s}, \hat{t}), \qquad y^u = \Gamma_3^u(\hat{s}, \hat{t}),$$

and

$$x^s = \Gamma_1^s(\hat{\sigma}, 0), \qquad \dot{x}^s = \Gamma_2^s(\hat{\sigma}, 0), \qquad y^s = \Gamma_3^s(\hat{\sigma}, 0).$$

Since $G(\hat{s}, \hat{t}, \hat{\sigma}) = 0$ we have that

$$x^u = x^s, \qquad \dot{x}^u = \dot{x}^s, \qquad \text{and} \qquad y^u = y^s. \tag{6}$$

Let

$$C_0 = E(\mathbf{x}_0),$$

denote the energy of the equilibrium. Then

$$E(x^u, \dot{x}^u, y^u, \Gamma_4^u(\hat{s}, \hat{t})) = E(x^s, \dot{x}^s, y^s, \Gamma_4^s(\hat{\sigma}, 0)) = C_0, \tag{7}$$

since stable/unstable manifolds have the same energy as $\mathbf{x}_0$. Recalling the formula for the Jacobi integral in Equation (4), Equation (7) becomes

$$\frac{1}{2}\left((\dot{x}^u)^2 + \Gamma_4^u(\hat{s}, \hat{t})^2\right) - \frac{1}{2}((x^u)^2 + (y^u)^2) - \frac{m_1}{r_1(x^u, y^u)} - \frac{m_2}{r_2(x^u, y^u)} - \frac{m_3}{r_3(x^u, y^u)} =$$

$$\frac{1}{2}\left((\dot{x}^s)^2 + \Gamma_4^s(\hat{\sigma}, 0)^2\right) - \frac{1}{2}((x^s)^2 + (y^s)^2) - \frac{m_1}{r_1(x^s, y^s)} - \frac{m_2}{r_2(x^s, y^s)} - \frac{m_3}{r_3(x^s, y^s)},$$

and employing the equalities of Equation (6) reduces this to

$$\Gamma_4^u(\hat{s}, \hat{t})^2 = \Gamma_4^s(\hat{\sigma}, 0)^2,$$

or

$$\Gamma_4^u(\hat{s}, \hat{t}) = \pm\Gamma_4^s(\hat{\sigma}, 0).$$

But $\Gamma_4^u(\hat{s}, \hat{t})$ and $\Gamma_4^s(\hat{\sigma}, 0)$ have the same sign by hypothesis, hence are equal. It follows that

$$\Gamma^u(\hat{s}, \hat{t}) = \Gamma^s(\hat{\sigma}, 0),$$

in all four components implying the orbit through $\hat{\mathbf{x}}$ is homoclinic to $\mathbf{x}_0$ as desired. □

The next lemma provides an a-posteriori condition for verifying the transversality condition is satisfied for a homoclinic orbit.

Lemma 1.5. *Suppose that $G\colon [-1,1]^3 \to \mathbb{R}^3$ is as in Lemma 1.4 and that $(\hat{s}, \hat{t}, \hat{\sigma}) \in (-1,1)^3$ has $G(\hat{s}, \hat{t}, \hat{\sigma}) = 0$. Assume in addition that $\Gamma_4^u(\hat{s}, \hat{t})$ and $\Gamma_4^s(\hat{\sigma}, 0)$ have the same sign, and let $\hat{\mathbf{x}} = \Gamma^u(\hat{s}, \hat{t}) = \Gamma^s(\hat{\sigma}, 0)$ denote the homoclinic point from Lemma 1.4. Assume that $DG(\hat{s}, \hat{t}, \hat{\sigma})$ is nonsingular, and that*

$$\nabla E(\hat{\mathbf{x}}) \neq 0.$$

Then the energy level set is a smooth 3-manifold near $\hat{\mathbf{x}}$, and the stable/unstable manifolds of $\mathbf{x}_0$ intersect transversally in the energy manifold.

Proof. Let

$$C_0 = E(\mathbf{x}_0),$$

once again denote the equilibrium energy and denote the energy level set of C_0 by

$$\mathcal{E}_0 := \left\{ \mathbf{x} \in \mathbb{R}^4 \, : E(\mathbf{x}) = C_0 \right\}.$$

It is an elementary fact from differential calculus (essentially the implicit function theorem) that if $\mathbf{x} \in \mathcal{E}_0$ is a regular point for E, then there exists an open neighborhood $V \subset \mathbb{R}^4$ of $\mathbf{x}$ so that $\mathcal{E}_0 \cap V$ is an embedded 3 dimensional disk (see for example Corollary 8.9 Chapter 8 of [60]). Since $E \colon U \subset \mathbb{R}^4 \to \mathbb{R}$ is real valued, $\mathbf{x}$ is a regular point if and only if

$$\nabla E(\mathbf{x}) \neq 0.$$

By assumption, $\nabla E(\hat{\mathbf{x}}) \neq 0$, and we conclude that $\mathcal{E}_0$ is a smooth three dimensional manifold near the homoclinic intersection point $\hat{\mathbf{x}}$. In particular, the tangent space of $\mathcal{E}_0$ is well defined at $\hat{\mathbf{x}}$, and has

$$\dim \left(T_{\hat{\mathbf{x}}} \mathcal{E}_0 \right) = 3.$$

Next, recall that by the stable manifold theorem $W^{s,u}(\mathbf{x}_0) \subset \mathbb{R}^4$ are themselves smooth 2-manifolds (as regular as f) and therefore, each has two dimensional tangent space at $\hat{\mathbf{x}}$. Moreover, $W^{s,u}(\mathbf{x}_0) \subset \mathcal{E}_0$ again by the continuity of E at $\mathbf{x}_0$ and thus, we claim that the tangent spaces of the stable/unstable manifolds at $\hat{\mathbf{x}}$ are linear subspaces of the tangent space of $\mathcal{E}_0$ at $\hat{\mathbf{x}}$. In other words: $W^{s,u}(\mathbf{x}_0)$ are embedded submanifolds near $\hat{\mathbf{x}}$.

To see this, define the embedded 2-disks

$$M_1 := \Gamma^u((-1,1)^2) \subset W^u(\mathbf{x}_0), \qquad \text{and} \qquad M_2 := \Gamma^s((-1,1)^2) \subset W^s(\mathbf{x}_0).$$

Note that $\hat{\mathbf{x}} \in M_1 \cap M_2$, by hypothesis. We will now argue that the tangent space of M_1 at $\hat{\mathbf{x}}$ is contained in the tangent space of $\mathcal{E}_0$ at $\hat{\mathbf{x}}$. The argument for M_2 is identical.

Choose $\eta \in T_{\hat{\mathbf{x}}} M_1$. Since $(\hat{s}, \hat{t}) \in (-1,1)^2$, there exists (by the definition of the tangent space/tangent vectors) an $\epsilon > 0$ and a curve $\gamma \colon (-\epsilon, \epsilon) \to \mathbb{R}^2$ satisfying

$$\gamma(0) = (\hat{s}, \hat{t}), \qquad \text{and} \qquad \gamma(\alpha) \in (-1,1)^2 \qquad \text{for all } \alpha \in (-\epsilon, \epsilon).$$

It follows that the curve $u \colon (-\epsilon, \epsilon) \to \mathbb{R}^4$ defined by

$$u(\alpha) := \Gamma^u(\gamma(\alpha)),$$

satisfies

$$\frac{d}{d\alpha} u(0) = \eta.$$

To obtain the desired containment we must show that η is in the tangent space of $\mathcal{E}_0$. To see this consider the function $g \colon (-\epsilon, \epsilon) \to \mathbb{R}$ defined by

$$g(\alpha) = E(\Gamma^u(\gamma(\alpha))),$$

and note that $g(\alpha) = C_0$ for all $\alpha \in (-\epsilon, \epsilon)$. Then we have

$$\begin{aligned} 0 &= \frac{d}{d\alpha} g(0) \\ &= \frac{d}{d\alpha} E(\Gamma^u(\gamma(0))) \\ &= \left\langle \nabla E(\Gamma^u(\gamma(0))), \frac{d}{d\alpha}\Gamma^u(\gamma(0)) \right\rangle \\ &= \langle \nabla E(u(0)), u'(0) \rangle \\ &= \langle \nabla E(\hat{\mathbf{x}}), \eta \rangle , \end{aligned}$$

so that

$$\eta \in \ker \nabla E(\hat{\mathbf{x}}).$$

However, the tangent space of the level set of a smooth real valued function coincides with the kernel of its gradient, so that

$$\eta \in T_{\hat{\mathbf{x}}} \mathcal{E}_0,$$

as desired.

Next, we establish the transversality. Define the vectors $\eta_1, \eta_2, \eta_3 \in \mathbb{R}^4$ by

$$\eta_1 = \partial_s \Gamma^u(\hat{s}, \hat{t}), \qquad \eta_2 = \partial_t \Gamma^u(\hat{s}, \hat{t}), \qquad \text{and} \qquad \eta_3 = -\partial_\sigma \Gamma^s(\hat{\sigma}, 0).$$

Since $\eta_1, \eta_2 \in T_{\hat{\mathbf{x}}} M_1$, and $\eta_3 \in T_{\hat{\mathbf{x}}} M_2$ it follows that $\eta_1, \eta_2, \eta_3 \in T_{\hat{\mathbf{x}}} \mathcal{E}_0$ by the discussion above. The hypothesis that $DG(\hat{s}, \hat{t}, \hat{\sigma})$ is nonsingular gives that its columns span $\mathbb{R}^3$. But the columns of $DG(\hat{s}, \hat{t}, \hat{\sigma})$ match the first three components of η_1, η_2, η_3, so that these three vectors are linearly independent in $T_{\hat{\mathbf{x}}} \mathcal{E}_0$. Recalling that $T_{\hat{\mathbf{x}}} \mathcal{E}_0$ is three dimensional, it follows that $\{\eta_1, \eta_2, \eta_3\}$ span $T_{\hat{\mathbf{x}}} \mathcal{E}_0$.

On the other hand, η_1, η_2 are linearly independent so they form a basis for $T_{\hat{\mathbf{x}}} M_1 = T_{\hat{\mathbf{x}}} W^u(\mathbf{x}_0)$. We claim that η_2, η_3 form a basis for $T_{\hat{\mathbf{x}}} M_2 = T_{\hat{\mathbf{x}}} W^s(\mathbf{x}_0)$ as well. To see this, recall that $\hat{\mathbf{x}} = \Gamma^s(\hat{\sigma}, 0) = \Gamma^s(\hat{s}, \hat{t})$ is the point of homoclinic intersection and note that

$$\partial_t \Gamma^s(\hat{\sigma}, 0) = \frac{1}{\tau_s} f(\Gamma^s(\hat{\sigma}, 0)),$$

as for $t \in (-1, 1)$ the curve $\Gamma^s(\hat{\sigma}, \tau_s t)$ is a solution of the differential equation. (Here we use that the charts $\Gamma^{s,u}$ are well aligned with the flow). Moreover

$$\partial_t \Gamma^u(\hat{s}, \hat{t}) = \frac{1}{\tau_u} f(\Gamma^u(\hat{s}, \hat{t})),$$

for the same reason. But then

$$\begin{aligned}\eta_2 &= \partial_t \Gamma^u(\hat{s},\hat{t}) \\ &= \frac{1}{\tau_u} f(\Gamma^u(\hat{s},\hat{t})) \\ &= \frac{1}{\tau_u} f(\hat{\mathbf{x}}) \\ &= \frac{\tau_s}{\tau_u}\frac{1}{\tau_s} f(\Gamma^s(\hat{\sigma},0)) \\ &= \frac{\tau_s}{\tau_u}\partial_t \Gamma^s(\hat{\sigma},0) \\ &= \frac{\tau_s}{\tau_u}\eta_1,\end{aligned}$$

so that

$$\begin{aligned}\text{span}\,(\eta_2,\eta_3) &= \text{span}\left(\partial_t\Gamma^u(\hat{s},\hat{t}), -\partial_\sigma\Gamma^s(\hat{\sigma},0)\right) \\ &= \text{span}\,(\partial_\tau\Gamma^s(\hat{\sigma},0), -\partial_\sigma\Gamma^s(\hat{\sigma},0)) \\ &= T_{\hat{\mathbf{x}}}M_2 \\ &= T_{\hat{\mathbf{x}}}W^s(\mathbf{x}_0),\end{aligned}$$

as claimed. Taken together, we have that η_1, η_2, η_3 simultaneously span the tangent spaces of the stable/unstable manifolds at $\hat{\mathbf{x}}$, and also span the tangent space of $\mathcal{E}_0$, which is to say that

$$T_{\hat{\mathbf{x}}}W^u(\mathbf{x}_0) \oplus T_{\hat{\mathbf{x}}}W^s(\mathbf{x}_0) = T_{\hat{\mathbf{x}}}\mathcal{E}_0.$$

In other words $W^{s,u}$ intersect transversally at $\hat{\mathbf{x}}$ as desired. □

The remainder of the paper is organized as follows. In Section 2 we state and prove the a-posteriori theorem which is the main tool for the computer assisted proof of Theorem 1.3. In Section 3 we review the parameterization method for invariant manifolds. In Section 4 we develop formal power series methods for solving the partial differential equations which appear in the parameterization method. First we make a change of variables which transforms the CRFBP to a polynomial system of seven (rather than four) differential equations. Mathematically rigorous error bounds for our invariant manifold computations are discussed in the companion paper [61] on the numerical implementation. It is reasonable to separate the discussion into two separate papers, as validating the truncation error estimates for the parameterization method has a distinctly infinite dimensional flavor. In Section **??** we show how the results of the earlier sections are combined to complete the proof of Theorem 1.3. The paper concludes with several appendices containing additional technical details which are omitted from the main sections for readability.

2 A finite dimensional a-posteriori existence theorem

Our approach to computer assisted proof is in the tradition of the work of Lanford, Eckmann, Wittwer, and Koch on renormalization theory and the Feigenbaum conjectures [62, 63, 64, 65]. The reader interested in more complete discussion of the literature in computer aided proofs in analysis might consult [66, 67, 68].

Throughout the section, let $\|\cdot\|$ denote any norm on $\mathbb{R}^n$, $\|\cdot\|_M$ denote the induced matrix norm, and $\|\cdot\|_Q$ denote the induced norm on bi-linear mappings. Explicit norms used in numerical applications are discussed in Appendix A. The following theorem, whose proof we include for the sake of completeness, is the main tool for the a-posteriori analysis described in the remainder of the paper.

Theorem 2.1. *Let $U \subset \mathbb{R}^n$ be an open set and assume $F\colon U \to \mathbb{R}^n$ is twice continuously differentiable. Suppose that $\bar{x} \in U$ and let $r_* > 0$ such that $\overline{B_{r_*}(\bar{x})} \subset U$. Assume A, $A^\dagger$ are $n \times n$ matrices, and Y_0, Z_0, Z_1, Z_2, are positive constants satisfying*

$$\|AF(\bar{x})\| \leq Y_0,$$

$$\left\|Id - AA^\dagger\right\|_M \leq Z_0,$$

$$\left\|A\left(A^\dagger - DF(\bar{x})\right)\right\|_M \leq Z_1,$$

and

$$\|A\|_M \sup_{x \in \overline{B_{r_*}(\bar{x})}} \|D^2F(x)\|_Q \leq Z_2.$$

Define the polynomial

$$p(r) := Z_2 r^2 - (1 - Z_0 - Z_1)r + Y_0,$$

and suppose $0 < r \leq r_*$ satisfies

$$p(r) < 0,$$

then there exists a unique $\hat{x} \in B_r(\bar{x})$ such that

$$F(\hat{x}) = 0.$$

Moreover $DF(\hat{x})$ is invertible and

$$\|DF(\hat{x})^{-1}\| \leq \frac{\|A\|}{1 - Z_2 r - Z_0 - Z_1}.$$

Proof. Assume the hypotheses of the theorem and suppose that there is an $0 < r \leq r_*$ so that $p(r) < 0$. Then

$$Z_2 r^2 + (Z_1 + Z_0)r + Y_0 < r, \tag{8}$$

from which we obtain

$$(Z_2 r + Z_1 + Z_0) + \frac{Y_0}{r} < 1.$$

Since all quantities are strictly positive we have that

$$\kappa := Z_2 r + Z_1 + Z_0 < 1,$$

and furthermore, $Z_0 < 1$. Then

$$\left\|\mathrm{Id} - AA^\dagger\right\|_M \leq Z_0 < 1,$$

and it follows by the Neumann theorem that the matrix $AA^\dagger$ is invertible. Then A and $A^\dagger$ are each invertible matrices, as an invertible matrix cannot factor through a singular matrix.

Now, define the *Newton-like* operator $T\colon U \to \mathbb{R}^n$ by

$$T(x) = x - AF(x).$$

Observe that since A is invertible, fixed points of T are in one to one correspondence with zeros of F. We show that T has a unique fixed point in $B_r(\bar{x})$ using Banach's fixed point theorem.

First note that

$$DT(x) = \mathrm{Id} - ADF(x), \qquad x \in U.$$

Since $\overline{B_r(\bar{x})} \subset U$, the formula holds throughout the closed set $\overline{B_r(\bar{x})}$. We estimate the derivative of T as follows. Let $x \in \overline{B_r(\bar{x})}$, then we have

$$\begin{aligned}
\|DT(x)\|_M &= \|\mathrm{Id} - ADF(x)\|_M \\
&\leq \|\mathrm{Id} - AA^\dagger\|_M + \|AA^\dagger - ADF(\bar{x})\|_M + \|ADF(\bar{x}) - ADF(x)\|_M \\
&\leq \|\mathrm{Id} - AA^\dagger\|_M + \left\|A\left(A^\dagger - DF(\bar{x})\right)\right\|_M + \|A\|_M \left(\sup_{y \in \overline{B_r(\bar{x})}} \|D^2F(y)\|_Q\right) \|x - \bar{x}\| \\
&\leq Z_0 + Z_1 + \|A\|_M \left(\sup_{y \in \overline{B_{r*}(\bar{x})}} \|D^2F(y)\|_Q\right) r \\
&\leq Z_0 + Z_1 + Z_2 r \\
&\leq \kappa.
\end{aligned}$$

Here we have used the second derivative bound of Lemma B.1 from Appendix A to pass from line two to three. The bound is uniform on $\overline{B_r(\bar{x})}$, and it follows that

$$\sup_{x \in \overline{B_r(\bar{x})}} \|DT(x)\| \leq \kappa < 1. \tag{9}$$

Next, we show that T maps $\overline{B_r(\bar{x})}$ into itself. To see this, let $x \in \overline{B_r(\bar{x})}$ and observe that

$$\begin{aligned}
\|T(x) - \bar{x}\| &\leq \|T(x) - T(\bar{x})\| + \|T(\bar{x}) - \bar{x}\| \\
&\leq \sup_{y \in \overline{B_r(\bar{x})}} \|DT(y)\|_M \|x - \bar{x}\| + \|AF(\bar{x})\| \\
&\leq (Z_2 r + Z_0 + Z_1) r + Y_0 \\
&< r,
\end{aligned}$$

where we have used Equation (8) in the last line. It follows that

$$T\left(\overline{B_r(\bar{x})}\right) \subset B_r(\bar{x}) \tag{10}$$

proving that T maps $\overline{B_r(\bar{x})}$ into itself (in fact the mapping is strictly into the interior).

Now for any $x_1, x_2 \in \overline{B_r(\bar{x})}$ we see that

$$\begin{aligned}
\|T(x_1) - T(x_2)\| &\leq \sup_{y \in \overline{B_r(\bar{x})}} \|DT(y)\|_M \|x_1 - x_2\| \\
&\leq \kappa \|x_1 - x_2\|,
\end{aligned}$$

with $\kappa < 1$. It follows that T is a strict contraction on $\overline{B_r(\bar{x})}$, which is a complete metric space, hence the Banach fixed point theorem implies that T has a unique fixed point, $\hat{x} \in \overline{B_r(\bar{x})}$. In fact, our inclusion from Equation (10) proves that $\hat{x} \in B_r(\bar{x})$. Recalling that fixed points of T correspond to zeros of F, we have that $\hat{x}$ is the unique zero of F in $B_r(\bar{x})$.

Finally, we show that $DF(\hat{x})$ is invertible. Define the matrix

$$B = -ADF(\hat{x}) + ADF(\bar{x}) - ADF(\bar{x}) + AA^\dagger - AA^\dagger + \mathrm{Id}.$$

Then, we have

$$\begin{aligned} ADF(\hat{x}) &= ADF(\hat{x}) - ADF(\bar{x}) + ADF(\bar{x}) - AA^\dagger + AA^\dagger - \mathrm{Id} + \mathrm{Id} \\ &= \mathrm{Id} - B. \end{aligned}$$

Moreover, we have the estimate

$$\begin{aligned} \|B\|_M &\leq \|ADF(\hat{x}) - ADF(\bar{x})\|_M + \|ADF(\bar{x}) - AA^\dagger\|_M + \|AA^\dagger - \mathrm{Id}\|_M \\ &\leq \|A(DF(\hat{x}) - DF(\bar{x}))\|_M + \|A(DF(\bar{x}) - A^\dagger)\|_M + \|AA^\dagger - \mathrm{Id}\|_M \\ &\leq \|A\|_M \sup_{y \in \overline{B_r(\bar{x})}} \|DF(y)\|_Q \, \|\hat{x} - \bar{x}\| + Z_1 + Z_0 \\ &\leq \|A\|_M \sup_{y \in \overline{B_{r_*}(\bar{x})}} \|DF(y)\|_Q \, r + Z_1 + Z_0 \\ &\leq Z_2 r + Z_1 + Z_0 \\ &= \kappa \\ &< 1, \end{aligned}$$

and it follows from another application of the Neumann theorem that $ADF(\hat{x}) = \mathrm{Id} - B$ is invertible. Hence, A and $DF(\hat{x})$ are each invertible. In fact, the Neumann theorem provides the bound

$$\|[ADF(\hat{x})]^{-1}\|_M = \|(\mathrm{Id} - B)^{-1}\|_M \leq \frac{1}{1 - \kappa}.$$

Multiplying on the right by A we obtain

$$DF(\hat{x})^{-1} = (\mathrm{Id} - B)^{-1} A,$$

and taking norms leads to the bound

$$\|DF(\hat{x})^{-1}\|_M \leq \frac{\|A\|_M}{1 - (Z_2 r + Z_0 + Z_1)},$$

which completes the proof. □

The following proposition provides an elementary application of Theorem 2.1 and also serves as the starting point for the invariant manifold computations leading to the main result in Section 5. A detailed proof including the derivation of each of the bounds required in 2.1 can be found in the companion paper [61].

Proposition 2.2 (Existence of a saddle-focus equilibrium in the CRFBP)**.** *Fix mass parameters* $m_1 = 0.5$*,* $m_2 = 0.3$*, and* $m_3 = 0.2$*, and let* f *denote the CRFBP vector field defined in Equation* (3)*. Then,*

$$\bar{\mathbf{x}} = \begin{pmatrix} 0.927099246135636 \\ 0 \\ 0.217703423699760 \\ 0 \end{pmatrix}$$

is an approximation of an isolated equilibrium for f *denoted by* $\mathbf{x}_0$ *and this approximation satisfies the bound*

$$\|\mathbf{x}_0 - \bar{\mathbf{x}}\| \leq 3 \times 10^{-15},$$

where the norm is the max-norm defined in Appendix A. Moreover, the Jacobian matrix, $Df(\mathbf{x}_0)$*, has four non-zero eigenvalues of the form*

$$\lambda = \pm\alpha \pm i\beta,$$

where

$$\alpha \in [0.86237485318926, 0.86237485318937],$$

and

$$\beta \in [0.99101767480653, 0.99101767480664].$$

In particular $\mathbf{x}_0$ *is a saddle-focus.*

Remark 2 (Eigendata for $Df(\mathbf{x}_0)$). In the present work, it is convenient to compute eigenvalues and eigenvectors for $Df(\mathbf{x}_0)$ using the formulas established in Lemma C.1. However, in many problems no such formulas are available. Nevertheless, one can use existing validated numerical methods to compute the eigendata and such algorithms are standard, for example, in the IntLab package. See [68] for more complete discussion.

Applying Theorem 2.1 to obtain a constructive proof of existence for an equilibrium solution complements the results of [28, 29]. These papers provide the correct possible count of equilibrium solutions of the CRFBP, while the computation described here allows one to compute the locations of these equilibria with tight, rigorous error bounds.

3 The parameterization method

The parameterization method is a functional analytic framework for studying invariant manifolds of discrete and continuous time dynamical systems. The works of [69, 70, 71, 72, 73, 74] developed the method for stable/unstable manifolds in Banach spaces, as well as for whiskered tori and their attached invariant manifolds. A review of the substantial literature surrounding the parameterization method is beyond the scope of the present work, and the interested reader can consult the book of [75] for examples, applications, and a thorough overview of the literature.

We begin by describing the parameterization method relevant to the setting in this work. It is worth emphasizing up front that the dynamics for the CRFBP are generated by the vector field on $\mathbb{R}^4$ given explicitly in Equation (3). However, this vector field is not amenable to many of the tools required in the proof of the main result, and we are forced to work with a higher dimensional vector field whose dynamics, restricted to an appropriate lower dimensional manifold, are equivalent to

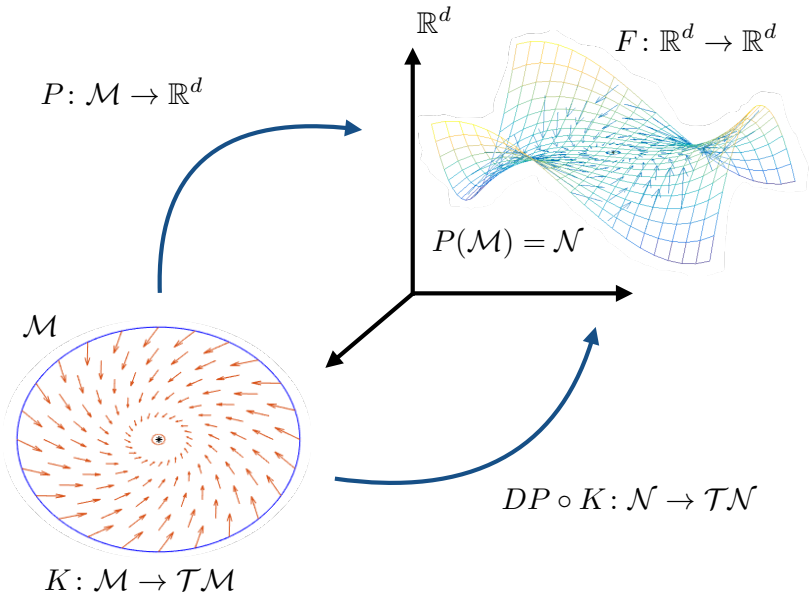

Figure 3: **Schematic illustration of the parameterization method**: $\mathcal{M}$ is a smooth manifold and P is an embedding. The vector field, K, is pushed forward by DP yielding a vector field, $DP \circ K$ on $\mathcal{N} = P(\mathcal{M})$. If the push forward vector field is equal to the restriction of F to $\mathcal{N}$, then the dynamics generated by these two vector fields are conjugate, $\mathcal{N}$ is a locally invariant manifold, and DP is an explicit conjugacy between the dynamics.

the CRFBP dynamics. For this reason, our development of the parameterization method will be slightly more general. The description of the (extended) CRFBP vector field and the discussion of its necessity are taken up in Section 4.1.

For the remainder of this section, we fix $d \in \mathbb{N}$, let $F\colon \mathbb{R}^d \to \mathbb{R}^d$ be a smooth vector field, $\mathcal{M}$ a smooth manifold of dimension $m \in \mathbb{N}$, and $P\colon \mathcal{M} \to \mathbb{R}^d$ a smooth embedding into $\mathbb{R}^d$ denoted by $\mathcal{N} = P(\mathcal{M})$. If $\mathcal{N}$ is a manifold with boundary, we additionally require that F is inflowing/outflowing on the boundary. Let $T\mathcal{M}$, $T\mathcal{N}$ denote the respective tangent bundles, then for $\sigma \in \mathcal{M}$ and $x \in \mathcal{N}$, we write $T_\sigma\mathcal{M}$ and $T_x\mathcal{N}$, to denote the tangent spaces based at σ and x respectively. Also, for any $\sigma \in \mathcal{M}$, the differential is a linear map from $T_\sigma\mathcal{M}$ to $T_{P(\sigma)}\mathcal{N}$ denoted by $DP(\sigma)$.

Now, suppose $K\colon \mathcal{M} \to T\mathcal{M}$ is a vector field on $\mathcal{M}$, define the vector field induced on the image of P by $DP(\sigma)K(\sigma) \in T_{P(\sigma)}\mathcal{N}$, and assume $P\colon \mathcal{M} \to \mathbb{R}^d$ satisfies the *invariance equation*

$$DP \circ K = F \circ P. \tag{11}$$

Then, the push forward of K is equal to the restriction of F on P and this restriction is everywhere tangent to the image of P. The situation is illustrated in Figure 3.

More specifically, let us introduce the coordinates, $\sigma = (\sigma_1, \ldots, \sigma_m)$ on $\mathcal{M}$, and denote the components of the vector field K by $K_1(\sigma)$, …, $K_m(\sigma)$. Then, we obtain explicit coordinates for

the push forward as

$$(DP \circ K)(\sigma) = K_1(\sigma)\frac{\partial}{\partial \sigma_1}P(\sigma) + \ldots + K_m(\sigma)\frac{\partial}{\partial \sigma_m}P(\sigma).$$

On the other hand, the restriction is given explicitly by

$$\left(F\,|_{\mathcal{N}}\right)(\sigma) = F(P(\sigma)),$$

and from our assumption that P satisfies Equation (11) we obtain the key identity

$$K_1(\sigma)\frac{\partial}{\partial \sigma_1}P(\sigma) + \ldots + K_m(\sigma)\frac{\partial}{\partial \sigma_m}P(\sigma) = F(P(\sigma)), \tag{12}$$

which holds for all $\sigma \in \mathcal{M}$. We describe how one obtains solutions to the invariance equation in the form of Equation (12) in the remainder of this section. For later reference, we note several important properties of these solutions:

- P maps orbits of K on $\mathcal{M}$ to orbits of F on $\mathcal{N}$. That is, the infinitesimal conjugacy of Equation (12) generates a flow conjugacy on the manifolds. This is made more precise in the examples in the next sections. The manifold $\mathcal{M}$ is referred to as the model space and the vector field K as the model dynamics.
- There is no requirement that P be the graph of a function, hence the parameterization can follow folds in the embedding.
- Equation (12) is a first order nonlinear system of PDEs, and provides a quantitative approach to the study of invariant manifolds. Note for example that Equation (12) depends only on the vector field F, and not on the implicitly defined flow which is unknown. In particular, P is the only quantity appearing in the equation which is not explicitly known.
- The fact that P solves a PDE is useful for both implementing numerical methods and for developing a-posteriori analysis.

3.1 Stable/Unstable manifolds attached to a saddle-focus

Throughout this section $z = x + iy$ denotes a complex number with $|z| = \sqrt{x^2 + y^2}$ the usual complex modulus. Relevant vector space norms used in the present work are discussed in detail in Appendix A. Let

$$D := \left\{\mathbf{z} = (z_1, z_2) \in \mathbb{C}^2 : |z_1|, |z_2| < 1\right\},$$

denote the open unit polydisc centered at the origin in $\mathbb{C}^2$.

Suppose $U \subset \mathbb{C}^d$ is an open set, $F\colon U \to \mathbb{C}^d$ is an analytic vector field, and $\mathbf{x}_0 \in U$ is a saddle-focus equilibrium for F. Specifically, we assume that $DF(\mathbf{x}_0)$ has complex conjugate eigenvalues, $\lambda_1, \lambda_2 \in \mathbb{C}$, with $\text{real}(\lambda_{1,2}) < 0$. Assume in addition that none of the other eigenvalues for $DF(\mathbf{x}_0)$ are stable, so that $W^s(\mathbf{x}_0)$ is two dimensional. Let $\xi_1, \xi_2 \in \mathbb{C}^d$ be eigenvectors associated with λ_1, λ_2 respectively.

Take $\mathcal{M} = D$ to be the model space for the stable manifold with the model dynamics generated by the linearization. In particular, we have the explicit expression for our model vector field, $K\colon D \to \mathbb{C}^2$, given by

$$K(\mathbf{z}) := \Lambda\mathbf{z} \qquad\qquad \mathbf{z} = (z_1, z_2) \in D,$$

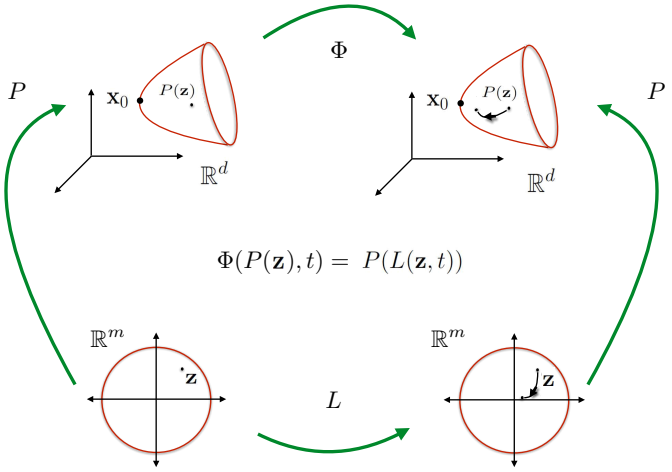

Figure 4: **Flow conjugacy:** If P is a solution to Equation (13), then P is a dynamical conjugacy mapping orbits of the linearized flow, L, to orbits of Φ, and the diagram above commutes.

where Λ is the 2-by-2 matrix

$$\Lambda = \begin{pmatrix} \lambda_1 & 0 \\ 0 & \lambda_2 \end{pmatrix}.$$

For this choice of our model problem, $P\colon D \to \mathbb{C}^d$ is a solution to Equation (12) if and only if P satisfies

$$\lambda_1 z_1 \frac{\partial}{\partial z_1} P(z_1, z_2) + \lambda_2 z_2 \frac{\partial}{\partial z_2} P(z_1, z_2) = F(P(z_1, z_2)), \tag{13}$$

for all $(z_1, z_2) \in D$, as well as the first order constraints

$$P(0,0) = \mathbf{x}_0, \qquad \frac{\partial}{\partial z_1} P(0,0) = s\xi_1, \qquad \text{and} \qquad \frac{\partial}{\partial z_2} P(0,0) = s\xi_2, \tag{14}$$

where $|s| > 0$ is an arbitrary nonzero scaling. Moreover, the following Lemma establishes that P is a conjugacy between the linear flow generated by K, and the nonlinear flow generated by F. The geometric significance of this Lemma is illustrated in Figure 4.

Lemma 3.1 (Flow conjugacy for the model dynamics)**.** *Suppose that $P\colon D \to \mathbb{C}^d$ is a smooth solution of the invariance equation* (13)*. Then for any $\mathbf{z} = (z_1, z_2) \in D$ and $t \geq 0$, P satisfies*

$$\Phi(P(\mathbf{z}), t) = \Phi(P(z_1, z_2), t) = P(e^{\lambda_1 t} z_1, e^{\lambda_2 t} z_2) = P\left(e^{\Lambda t} \mathbf{z}\right). \tag{15}$$

Proof. Choose $(z_1, z_2) \in D$, and define the curve $\gamma\colon [0, \infty) \to \mathbb{C}^d$ by

$$\gamma(t) = P(e^{\lambda_1 t} z_1, e^{\lambda_2 t} z_2).$$

Note that γ is well defined since by assumption $\text{real}(\lambda_{1,2}) < 0$ and therefore

$$(e^{\lambda_1 t} z_1, e^{\lambda_2 t} z_2) \in D, \qquad \text{for all } t \in [0, \infty). \tag{16}$$

Combining the result in Equation (16) with the hypothesis that P satisfies Equation (13) on D, it follows that

$$F\left(P(e^{\lambda_1 t}z_1, e^{\lambda_2 t}z_2)\right) = \lambda_1\left(e^{\lambda_1 t}z_1\right)\frac{\partial}{\partial z_1}P(e^{\lambda_1 t}z_1, e^{\lambda_2 t}z_2) + \lambda_2\left(e^{\lambda_2 t}z_2\right)\frac{\partial}{\partial z_2}P(e^{\lambda_1 t}z_1, e^{\lambda_2 t}z_2). \quad (17)$$

holds for all $t > 0$. On the other hand,

$$\begin{aligned}
\frac{d}{dt}\gamma(t) &= \frac{d}{dt}P(e^{\lambda_1 t}z_1, e^{\lambda_2 t}z_2) \\
&= DP(e^{\lambda_1 t}z_1, e^{\lambda_2 t}z_2)\begin{pmatrix} \lambda_1 e^{\lambda_1 t}z_1 \\ \lambda_2 e^{\lambda_2 t}z_2 \end{pmatrix} \\
&= \lambda_1\left(e^{\lambda_1 t}z_1\right)\frac{\partial}{\partial z_1}P(e^{\lambda_1 t}z_1, e^{\lambda_2 t}z_2) + \lambda_2\left(e^{\lambda_2 t}z_2\right)\frac{\partial}{\partial z_2}P(e^{\lambda_1 t}z_1, e^{\lambda_2 t}z_2) \\
&= F(P(e^{\lambda_1 t}z_1, e^{\lambda_2 t}z_2)) \\
&= F(\gamma(t)),
\end{aligned}$$

where we have used Equation (17) to pass from the third to the fourth line. We also note that $\gamma(0) = P(\mathbf{z})$, and it follows that γ satisfies the initial value problem $\gamma' = F(\gamma)$ with initial data $\gamma(0) = P(\mathbf{z})$. Equivalently, γ is a parameterization of the trajectory of Φ through $(\mathbf{z})$, and it follows that

$$\Phi(P(\mathbf{z}), t) = \gamma(t) = P(e^{\lambda_1 t}z_1, e^{\lambda_2 t}z_2),$$

for all $t \geq 0$. Since $\mathbf{z} \in D$ was arbitrary we have the result. □

Upon examination of the conjugacy in Lemma 3.1, it becomes clear that P parameterizes a local stable manifold of $\mathbf{x}_0$. Specifically, P is continuous and therefore, for every $\mathbf{z} \in D$ we have

$$\begin{aligned}
\lim_{t\to\infty}\Phi\left(P(\mathbf{z}), t\right) &= \lim_{t\to\infty}P\left(e^{\Lambda t}\mathbf{z}\right) \\
&= P\left(\lim_{t\to\infty}e^{\Lambda t}\mathbf{z}\right) \\
&= P(0).
\end{aligned}$$

Recalling the first order constraints in Equation (14), we have $P(0) = \mathbf{x}_0$ and it follows that

$$P(D) \subset W^s(\mathbf{x}_0).$$

Finally, we remark that the preceding discussion and results apply for unstable manifolds by reversing time.

Remark 3 (Real parameterizations for real analytic vector fields). In this work we are interested in the two-dimensional stable/unstable manifolds for a saddle-focus type equilibrium in the (extended) CRFBP vector field. Specifically, we are only interested in the case where F is a vector field on $\mathbb{R}^d$, and thus, in addition to satisfying Equations (13) and (14), we require P to parameterize the *real* invariant manifold (i.e. P should take values in $\mathbb{R}^d$). While not apparent from the discussion above, this requirement places no additional constraints on P, and such a condition can always

be satisfied. To see this, we consider P as in Lemma 3.1 which we assume is given by the Taylor expansion

$$P(z_1, z_2) = \sum_{m=0}^{\infty} \sum_{n=0}^{\infty} a_{mn} z_1^m z_2^n \qquad a_{mn} \in \mathbb{C}^d.$$

Additionally, assume the coefficients for P satisfy the conjugate symmetry condition

$$a_{mn} = \text{conj}(a_{nm}) \qquad \text{for all} \quad (m, n) \in \mathbb{N}^2,$$

where $\text{conj}(z)$ denotes complex conjugation. Then, for every $z \in \{z \in \mathbb{C} : |z| < 1\}$, we have $P(z, \text{conj}(z)) \in \mathbb{R}^d$ (in fact this is equivalent to the conjugate symmetry condition). Now, we denote the unit disc in $\mathbb{R}^2$ by

$$B := \left\{ (\sigma_1, \sigma_2) \in \mathbb{R}^2 : \sqrt{\sigma_1^2 + \sigma_2^2} < 1 \right\},$$

and it follows that if $|z| < 1$, we may parameterize $(z, \text{conj}(z)) \in D$ through B by setting

$$z = \sigma_1 + i\sigma_2 \quad \text{and} \quad \text{conj}(z) = \sigma_1 - i\sigma_2 \qquad \text{for some} \quad (\sigma_1, \sigma_2) \in B.$$

In other words, if P satisfies the conjugate symmetry condition, then $P \colon B \to \mathbb{R}^d$ is a real parameterization of the two-dimensional stable manifold as required. As in the previous discussion, the result is similar for the unstable manifold.

To see that the conjugate symmetry condition for the coefficients can always be satisfied, recall that $\lambda_1 = \text{conj}(\lambda_2)$, implying that if ξ_1 is any eigenvector for λ_1, then $\text{conj}(\xi_1)$ is an eigenvector for λ_2. The coefficients for P are uniquely determined only up to eigenvector scaling which we are free to choose. By inspection of the first order data in Equation (14), we see that if ξ_1 is our chosen (scaled) eigenvector for λ_1, then choosing $\xi_2 = \text{conj}(\xi_1)$ ensures that the coefficients of P satisfy the conjugate symmetry condition to first order.

By an inductive argument, it can be proved that if P satisfies this condition to first order, then it satisfies the condition to all orders which justifies our claim that P can be assumed to satisfy the conjugate symmetry condition. The reader interested in the full details is referred to [27, 76] for a complete proof for (resonance free) invariant manifolds in arbitrary dimensions and [77] for an in depth analysis of the relationship between local parameterizations for different choices of eigenvector scaling.

Remark 4 (Existence and uniqueness of solutions of Equation (13)). Existence, uniqueness, and regularity questions concerning the parameterization method for stable/unstable manifolds of equilibria are considered at length in [69, 70, 71, 73, 78]. For example, it can be shown that solutions (if they exist) are unique up to the choice of the eigenvector scalings, and that (if it exists) the parameterization, P, is as smooth as F i.e. P is analytic in the present case. Existence issues are more subtle, and involve certain *non-resonance* conditions between eigenvalues of like stability. See [69, 71, 75, 77] for precise definition of the resonance conditions and fuller discussion.

At present we only remark that in the case of a two dimensional saddle-focus, all subtleties concerning existence vanish. This is because a single pair of complex conjugate eigenvalues cannot be resonant in the relevant sense. For the manifolds studied in the present work we have the following result. Let ξ_1, ξ_2 denote some choice of eigenvectors as in the above discussion, and $s \neq 0$. Then, there exists an $\epsilon > 0$ so that for all $|s| < \epsilon$, there exists a unique, analytic solution to equation (13), which satisfies the first order constraints in Equation (14). Note that s is the eigenvector scaling parameter discussed above. For the analytic case, the proof is a consequence of the implicit function theorem, see for example [71].

3.2 Advection of transverse arcs

In this section, we describe the use of rigorous advection to pass from a single local parameterization of an invariant manifold to an atlas of analytic chart maps which parameterize the global manifold. Recall that in our setting, $F\colon \mathbb{R}^d \to \mathbb{R}^d$, denotes a real analytic vector field, and suppose that $\gamma\colon [-1,1] \to \mathbb{R}^d$ is a real analytic curve which is transverse to the vector field. Specifically, we require that

$$\langle \gamma'(s), F(\gamma(s)) \rangle \neq 0,$$

for all $s \in [-1,1]$ where $\langle \cdot, \cdot \rangle$ is the Euclidean inner product (actually it is reasonable to allow the inner product to vanish at ± 1 only if $F(\gamma(\pm 1)) = 0$). Under this transversality condition, the advected curve is a locally invariant manifold, which we can describe in the language of the previous section.

As in Section 3.1, we choose a model space to work in with dynamics which are understood. In particular, we take $\mathcal{M} = [-1,1]^2$ as our model space, and for fixed $|\tau| > 0$, our model dynamics are generated by the "flow box" vector field, $K\colon [-1,1]^2 \to \mathbb{R}^2$, defined by

$$K(s,t) = \begin{pmatrix} 0 \\ \tau \end{pmatrix}.$$

Obtaining a parameterization for the advected image of γ is equivalent to finding a parameterization, $\Gamma\colon [-1,1]^2 \to \mathbb{R}^d$, which satisfies the invariance equation for the model problem. Recalling Equation (12), we have that Γ must satisfy

$$\tau \frac{\partial}{\partial t} \Gamma(s,t) = F(\Gamma(s,t)) \qquad \Gamma(s,0) = \gamma(s). \tag{18}$$

This equation amounts to the statement that Γ solves the usual initial value problem for the curve of initial conditions parameterized by γ, and we include it only to emphasize the fact that the parameterization obtained is well aligned with the flow in the sense discussed in Section 1.2.

Finally, we note that one chooses $\tau < 0$ when advecting the stable manifold, and $\tau > 0$ when advecting the unstable manifold, so that in each case the local invariant manifold becomes larger under advection.

3.3 Growing the atlas

For the current setting, let $B \subset \mathbb{R}^2$ denote the open unit disk in the plane, and suppose that $P\colon B \to \mathbb{R}^d$ is a real valued parameterization of a local (un)stable manifold attached to a saddle-focus equilibrium, $\mathbf{x}_0$, as discussed in Section 3.1. Let $\mathbf{c}_j\colon [-1,1] \to B$, $1 \leq j \leq M$ denote a system of real analytic arcs, continuous on the closed interval, with $\mathbf{c}_1(-1) = \mathbf{c}_M(1)$, so that $C := \cup_{j=1}^{M} c_j([-1,1])$ is a closed loop. Moreover, assume that C has no self intersections, and has winding number 1 with respect to the origin in B. Finally, suppose that the vector field generated by $\mathcal{M}$ is nowhere tangent to C. That is, the vector field is inflowing/outflowing with respect to C, so that the interior of the region bounded by C defines a fundamental domain for the stable/unstable manifold. Then

$$\gamma = \bigcup_{j=1}^{M} P(c_j(s)),$$

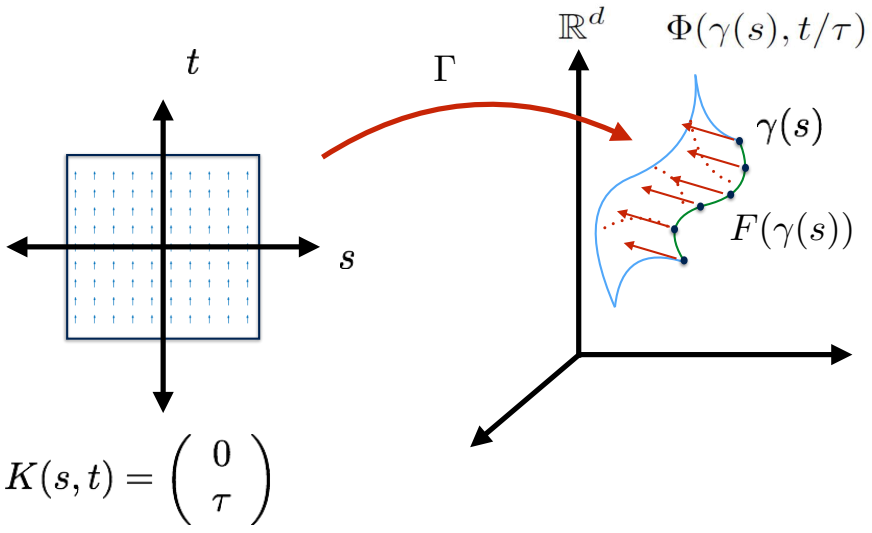

Figure 5: **Parameterization of an advected curve:** $\mathcal{M} = [-1,1]^2$ is our model space and the constant vector field $K(s,t) = (0,\tau)$ generates the model dynamics. Solving the invariance equation $DP \circ K = F(P)$ leads to a parameterization of the locally invariant manifold given by advecting γ. The dynamics are conjugate to the flow box dynamics on $\mathcal{M}$. That is $P(s,t) = \Phi(\gamma(s), t/\tau)$.

is an inflowing/outflowing boundary for a local (un)stable manifold of $\mathbf{x}_0$. In other words, for $1 \leq j \leq M$, $\gamma_j = P \circ c_j$ is an arc segment on the (un)stable manifold boundary which is everywhere transverse to the vector field, F. It follows that the advected images of these sub-arcs are analytic charts of the form

$$\Gamma_j(s,t) = \Phi(\gamma_j(s), t),$$

whose images lie in the global (un)stable manifold. In fact,

$$P(B) \cup \bigcup_{j=1}^{M} \Gamma_j([-1,1]^2),$$

is an analytic continuation of the local (un)stable manifold. The idea is illustrated in Figure 6.

Now, this collection of $(M+1)$ charts is an atlas for a (larger) local (un)stable manifold for $\mathbf{x}_0$. Moreover, we define

$$\gamma_j^1(s) = \Gamma_j(s,1) \qquad 1 \leq j \leq M,$$

and we obtain a parameterization of the boundary of the larger local (un)stable manifold which we note is again transverse to the flow. Thus, the procedure is repeated with this new boundary as the initial data. In this way, we systematically "grow" an increasingly large local portion of the (un)stable manifold of $\mathbf{x}_0$.

Remark 5 (Remeshing). A typical arc segment advected by a nonlinear flow undergoes rapid deformation and stretching. Thus, during the advection procedure, it frequently happens that the

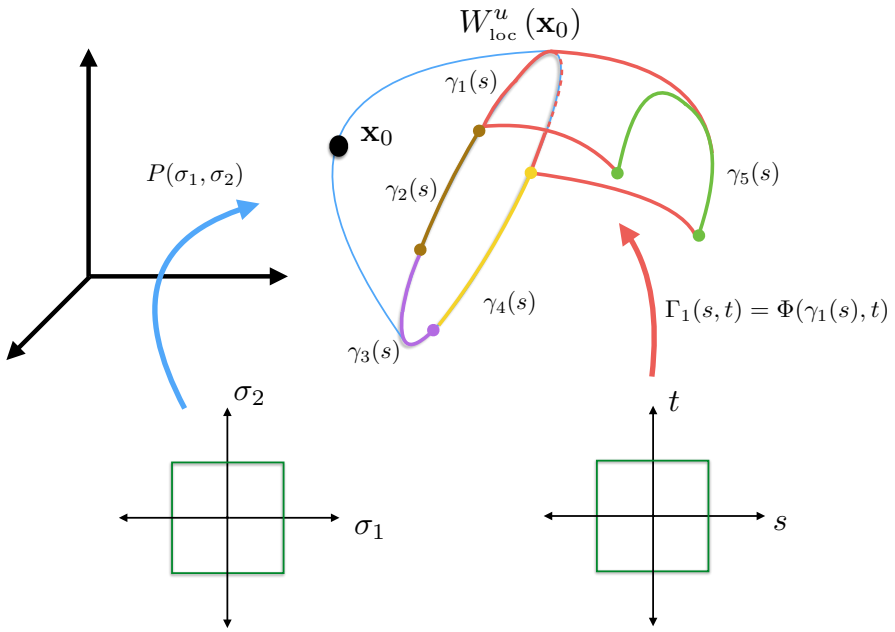

Figure 6: Two kinds of charts comprising the atlas. P is a local patch containing the saddle-focus which is computed using the parameterization method discussed in Section 3.1. Next, the boundary of $\mathcal{M}$ is meshed into sub-arcs and lifted through P to obtain a parameterization of the local manifold boundary. A larger local manifold is "grown" by advecting these boundary arcs yielding a collection of charts which parameterizes the manifold far from the equilibrium.

length or curvature of the arc, $\Gamma_j(s, 1)$, is an order of magnitude larger (or more), than the initial arc $\gamma_j(s)$. In this case, it is desirable to subdivide γ_j into an appropriate number of smaller arcs before continuing to advect it. This remeshing is one of the most delicate parts of the procedure as this deformation is difficult to predict. However, heuristics based on tools from numerical analysis allow this rigorous advection to be carried out much longer than we require in the present work. We use the adaptive scheme developed in [25], and refer the interested reader to that reference for more detailed discussion of these considerations.

4 Formal series expansions

In this section we develop formal series expansions for the invariant manifold parameterizations described in the previous section. Recalling our remarks in that section, we will not work with the vector field in Equation (3). Instead, we first develop the *extended* CRFBP vector field which is defined on $\mathbb{R}^7$. This vector field is derived by a procedure we refer to as automatic differentiation. For the current work, the significance of the automatic differentiation is the fact that the resulting vector field is polynomial which is crucial for the application of the rigorous numerical methods

employed in the proof of the main result. The trade-off is that the dimension of the relevant vector field increases which presents two complications.

The first is the increased complexity and decreased numerical stability of the algorithmic implementations which produce the rigorous (un)stable manifold parameterizations using the methods described in Section 3. Given its distinctly computational flavor, further discussion of this problem is deferred to the companion paper [61] which focuses exclusively on implementation details and computational algorithms.

However, automatic differentiation causes an additional, purely mathematical complication. Namely, in what sense do the dynamics of the extended vector field correspond to the dynamics in the 4-dimensional "true" CRFBP? In this section, we address this concern explicitly for the CRFBP. However, the results are widely applicable to general analytic vector fields which extend (through automatic differentiation) to a polynomial vector field.

4.1 A polynomial problem related to the CRFBP: Automatic Differentiation

The idea of the automatic differentiation is to introduce new variables

$$u_5 = \frac{1}{r_1}, \quad u_6 = \frac{1}{r_2}, \quad \text{and} \quad u_7 = \frac{1}{r_3},$$

where the r_j, for $j = 1, 2, 3$ are as defined in Equation (2). The new variables capture the non-polynomial nonlinearity of the CRFBP and are incorporated into the vector field by *appending* their time derivatives. Specifically, observe that

$$\begin{aligned} u_5' &= \frac{-1}{r_1^2} r_1' \\ &= \frac{-1}{r_1^2} \frac{d}{dt} \sqrt{(x(t)-x_1)^2 + (y(t)-y_1)^2} \\ &= \frac{-1}{r_1^2} \frac{\frac{d}{dt}(x(t)-x_1)^2 + (y(t)-y_1)^2}{2\sqrt{(x(t)-x_1)^2 + (y(t)-y_1)^2}} \\ &= -(u_1 - x_1)u_2 u_5^3 - (u_3 - y_1)u_4 u_5^3. \end{aligned}$$

Similar calculations show that differentiating r_6 and r_7 leads to the equations

$$\begin{aligned} u_6' &= -(u_1 - x_2)u_2 u_6^3 - (u_3 - y_2)u_4 u_6^3, \\ u_7' &= -(u_1 - x_3)u_2 u_7^3 - (u_3 - y_3)u_4 u_7^3. \end{aligned}$$

Expressed in these new variables, the partials of Ω are

$$\begin{aligned} \Omega_x &= u_1 - m_1(u_1 - x_1)u_5^3 - m_2(u_1 - x_2)u_6^3 - m_3(u_1 - x_3)u_7^3, \\ \Omega_y &= u_3 - m_1(u_3 - y_1)u_5^3 - m_2(u_3 - y_2)u_6^3 - m_3(u_3 - y_3)u_7^3, \end{aligned}$$

and letting $\mathbf{u} = (u_1, u_2, u_3, u_4, u_5, u_6, u_7) \in \mathbb{C}^7$ denote the new vector of variables, we study the extended differential equation

$$\mathbf{u}' = F(\mathbf{u}),$$

where $F\colon \mathbb{C}^7 \to \mathbb{C}^7$, is a polynomial vector field. Specifically, the extended CRFBP vector field is given explicitly by the formula

$$F(\mathbf{u}) = \begin{pmatrix} u_2 \\ 2u_4 + u_1 - m_1 u_1 u_5^3 + m_1 x_1 u_5^3 - m_2 u_1 u_6^3 + m_2 x_2 u_6^3 - m_3 u_1 u_7^3 + m_3 x_3 u_7^3 \\ u_4 \\ -2u_2 + u_3 - m_1 u_3 u_5^3 + m_1 y_1 u_5^3 - m_2 u_3 u_6^3 + m_2 y_2 u_6^3 - m_3 u_3 u_7^3 + m_3 y_3 u_7^3 \\ -u_1 u_2 u_5^3 + x_1 u_2 u_5^3 - u_3 u_4 u_5^3 + y_1 u_4 u_5^3 \\ -u_1 u_2 u_6^3 + x_2 u_2 u_6^3 - u_3 u_4 u_6^3 + y_2 u_4 u_6^3 \\ -u_1 u_2 u_7^3 + x_3 u_2 u_7^3 - u_3 u_4 u_7^3 + y_3 u_4 u_7^3 \end{pmatrix}. \tag{19}$$

Remark 6 (The dynamics of automatic differentiation). Taylor series methods for numerical integration of N-body problems has a long history. Examples going back to the 1950s and 1960s can be found in the works of [79, 80, 81], where one finds automatic differentiation schemes similar to the one proposed by us in this section. However, it is important to note that the authors of the works just cited consider only initial value problems for point data, as opposed to smooth manifolds of initial conditions. Additionally, replacing the given system with a polynomial system is not rigorously justified in these works and additional care must be taken to obtain rigorous theorems when applying automatic differentiation.

We note that other approaches to automatic differentiation work directly with the power series for the nonlinear terms, without introducing first an auxiliary polynomial vector field. See for example Chapter 4.6 of [82] and also the discussion in [75]. One advantage of our approach is that it generalizes to other spectral bases such as Fourier [41] and Chebyshev series [83, 84]. Another advantage is that one only has to implement the validated manifold computations for polynomial vector fields.

4.2 Recovering the CRFBP from the polynomial problem

In this section, we analyze the relationship between the CRFBP dynamics generated by f, defined in Equation (3), and the extended CRFBP generated by F as defined in Equation (19). Specifically, we prove an explicit forcing theorem which gives sufficient conditions for the dynamics in the extended system to imply the existence of a transverse homoclinic for a saddle-focus in the original CRFBP.

The main complication is that the dynamics of f and F are not equivalent. For example, f has singularities, while F is a polynomial and hence entire. To justify the use of automatic differentiation, we show that by restricting to an appropriate four dimensional sub-manifold of $\mathbb{R}^7$ we recover the dynamics of f from those of F.

To make this more precise, we begin with several definitions. Define the *collision-free* set for f by

$$U := \left\{(x, \dot{x}, y, \dot{y}) \in \mathbb{C}^4 \,:\, (x, y) \neq (x_j, y_j) \text{ for } j = 1, 2, 3\right\}, \tag{20}$$

and note that f is analytic on U. Now, define the nonlinear map, $R\colon U \to \mathbb{C}^7$, by

$$R(x,\dot{x},y,\dot{y}) := \begin{pmatrix} x \\ \dot{x} \\ y \\ \dot{y} \\ \frac{1}{\sqrt{(x-x_1)^2+(y-y_1)^2}} \\ \frac{1}{\sqrt{(x-x_2)^2+(y-y_2)^2}} \\ \frac{1}{\sqrt{(x-x_3)^2+(y-y_3)^2}} \end{pmatrix}. \tag{21}$$

For $\mathbf{u} = (u_1, u_2, u_3, u_4, u_5, u_6, u_7) \in \mathbb{C}^7$, we define the subspace projections, $\pi\colon \mathbb{C}^7 \to \mathbb{C}^4$, and $\pi^\perp\colon \mathbb{C}^7 \to \mathbb{C}^3$, by

$$\pi(\mathbf{u}) = \begin{pmatrix} u_1 \\ u_2 \\ u_3 \\ u_4 \end{pmatrix}, \qquad \text{and} \qquad \pi^\perp(\mathbf{u}) = \begin{pmatrix} u_4 \\ u_5 \\ u_7 \end{pmatrix},$$

so that we have the decomposition $\mathbf{u} = (\pi(\mathbf{u}), \pi^\perp(\mathbf{u}))$. Observe that for any $\mathbf{x} \in \mathbb{C}^4$, R and π satisfy the identity

$$\pi(R(\mathbf{x})) = \mathbf{x}.$$

Now define the set

$$\mathcal{S} := \left\{\mathbf{u} \in \mathbb{C}^7 \,:\, \mathbf{u} = R(\mathbf{x}) \text{ for some } \mathbf{x} \in U \subset \mathbb{C}^4\right\} = R(U),$$

and observe that R is injective since $\mathbf{u} \in \mathcal{S}$ if and only if

$$\mathbf{u} = R(\pi\mathbf{u}). \tag{22}$$

Finally, we note the identity

$$\pi F(R(\mathbf{x})) = f(\mathbf{x}), \tag{23}$$

which says that the composition of F with R recovers the CRFBP field as its first four components.

We are interested in the relationship between the dynamics generated by the vector fields f and F. In particular, we want to prove that R lifts the dynamics generated by f on U, to dynamics generated by F restricted to $\mathcal{S}$. We begin with the identity

$$DR(\mathbf{x})f(\mathbf{x}) = F(R(\mathbf{x})) \qquad x \in U, \tag{24}$$

which follows from a straight-forward computation. In fact, one shows that this identity respects our subspace decomposition in the sense that

$$\begin{aligned} \pi DR(\mathbf{x})f(\mathbf{x}) &= \pi F(R(\mathbf{x})) \\ \pi^\perp DR(\mathbf{x})f(\mathbf{x}) &= \pi^\perp F(R(\mathbf{x})) \end{aligned} \tag{25}$$

for $\mathbf{x} \in U$.

We note that Equation (24) is the crucial identity which motivates the definition of R. Geometrically, Equation (24) says that the push forward of f by DR is equal to F on $\mathcal{S}$, which explains why the dynamics of F restricted to $\mathcal{S}$ recover the dynamics of f. In other words, Equation (24) is

an the infinitesimal dynamical conjugacy which provides a high level explanation of why automatic differentiation works and there is a one-to-one correspondence between the equilibria, eigenspaces, stable/unstable manifolds, and connecting orbits of f defined on U, and F restricted to $\mathcal{S} = R(U)$.

Moreover, Equations (23) and (25) provide the mathematical justification for studying the dynamics for f by studying the dynamics for F and "discarding" the appended coordinates. It says that the dynamics of f are recovered by projecting orbits of F onto their first four components. We make this conjugacy precise with the following theorem.

Theorem 4.1 (Dynamical forcing theorem for the extended CRFBP system)**.** *Suppose $\mathbf{x}_0$ is a saddle-focus equilibrium solution for f, so that $Df(\mathbf{x}_0)$ admits two pairs of non-zero, complex conjugate eigenvalues which have the form*

$$\lambda^s_{1,2} = -\alpha \pm i\beta, \qquad \lambda^u_{1,2} = \alpha \pm i\beta, \qquad \alpha, \beta > 0.$$

1. *(Orbit correspondence) Let Φ denote the flow generated on $\mathbb{C}^7$ by F, Ψ denotes the flow generated on U by f, and suppose $\mathbf{x} \in U$. Then, $\Phi(R(\mathbf{x}), t) = R\left(\Psi(\mathbf{x}, t)\right)$ for all t such that $\Psi(\mathbf{x}, t) \in U$. In particular, $\mathbf{u}_0 = R(\mathbf{x}_0) \in \mathbb{R}^7$, is an equilibrium solution for F.*

2. *(Linear stability) Let $\lambda \in \mathbb{C}$ denote an eigenvalue for $Df(\mathbf{x}_0)$ with $\xi \in \mathbb{C}^4$ an associated eigenvector. Then, λ is also an eigenvalue for $DF(\mathbf{u}_0)$ with*

$$\boldsymbol{v} = DR(\mathbf{x}_0)\xi \in \mathbb{C}^7,$$

   an associated eigenvector. Moreover, the remaining eigenvalues for $DF(\mathbf{u}_0)$ are all zero.

3. *(Invariant manifolds) Let $\xi^s_{1,2}$ denote the eigenvectors for $Df(\mathbf{x}_0)$ associated with the stable eigenvalues, $\lambda^s_{1,2}$. Then, the eigenvectors defined by*

$$\mathbf{v}^s_{1,2} = DR(\mathbf{x}_0)\xi^s_{1,2},$$

   span the local stable manifold attached to $\mathbf{u}_0$. Suppose that $P\colon D \to \mathbb{C}^7$ solves the invariance equation (13), subject to the first order constraints, $P(0) = \mathbf{u}_0$, $\partial_1 P(0) = \mathbf{v}^s_1$, and $\partial_2 P(0) = \mathbf{v}^s_2$, and assume that $\pi \circ P(D) \subset U$. Then, $p\colon D \to \mathbb{C}^4$ defined by

$$p(\mathbf{z}) = \pi P(\mathbf{z}) \qquad\qquad (\mathbf{z}) \in D,$$

   parameterizes a local stable manifold attached to $\mathbf{x}_0$ for the CRFBP. As usual, a similar result holds for the unstable manifold by substituting the unstable eigenvalues/eigenvectors.

We note that the result in Theorem 4.1 is, in fact, another instance of the invariance equation (11). Thus, the proof of the theorem, which is outlined in Appendix D, follows from arguing as in the proof of Lemma 3.1. This result suggests the following general strategy for obtaining rigorous results for non-polynomial vector fields via automatic differentiation.

Given an open set, $U \subset \mathbb{R}^d$, and a non-polynomial vector field, $f : U \to \mathbb{R}^d$, one seeks an embedding, $R\colon U \to \mathbb{R}^D$, and a polynomial vector field, $F\colon \mathbb{R}^D \to \mathbb{R}^D$, such that $\pi \circ R = \mathrm{Id}$, and Equation (24) is satisfied. Here, $\pi : \mathbb{R}^D \to \mathbb{R}^d$ is projection onto the first d-many coordinates. Note that these two properties automatically imply the critical identity in Equation 23. From these properties, one concludes that the dynamics of f on U are conjugate to the dynamics of F restricted to the graph of R, and in particular, $R(U)$ is an invariant manifold for F.

Of particular interest is the case where f is composed of finite sums, products, and compositions of elementary functions. In this case, the informal procedure of defining new variables and appending their derivatives, described in Section 4.1, naturally leads to an appropriate choice for F and R. For further discussion of automatic differentiation see [75].

4.3 Stable/unstable manifold of a saddle-focus

With the result of Theorem 4.1 in hand, we restrict our attention to the extended vector field for the remainder of this paper. Let $\mathbf{u}_0 \in \mathbb{R}^7$ be a saddle-focus equilibrium solution for F, $\lambda_1, \lambda_2 \in \mathbb{C}$ are complex conjugate eigenvalues for $DF(\mathbf{u}_0)$ (either stable or unstable), and let $\xi_1, \xi_2 \in \mathbb{C}^7$ be their associated eigenvectors. We look for a formal power series

$$P(z_1, z_2) = \sum_{m=0}^{\infty} \sum_{n=0}^{\infty} a_{mn} z_1^m z_2^n \qquad a_{mn} \in \mathbb{C}^7,$$

such that P is a solution of Equation (13). The first order constraints given in Equation (14) are satisfied by taking

$$a_{00} = \mathbf{u}_0, \qquad a_{10} = \xi_1, \qquad \text{and} \qquad a_{01} = \xi_2.$$

To obtain the higher order Taylor coefficients of P, we expand the left hand side of Equation (13) as a power series yielding

$$\lambda_1 z_1 \frac{\partial}{\partial z_1} P(z_1, z_2) + \lambda_2 z_2 \frac{\partial}{\partial z_2} P(z_1, z_2) = \sum_{m=0}^{\infty} \sum_{n=0}^{\infty} (m\lambda_1 + n\lambda_2) a_{mn} z_1^m z_2^n. \tag{26}$$

For the right hand side of Equation (13), we assume we have a power series expansion for the composition in the form

$$F(P(z_1, z_2)) = \sum_{m=0}^{\infty} \sum_{n=0}^{\infty} b_{mn} z_1^m z_2^n. \tag{27}$$

Equating the expression in (26) with (27) and matching like powers, we obtain countably many vector valued equations

$$(m\lambda_1 + n\lambda_2) a_{mn} = b_{mn}. \tag{28}$$

Since F is polynomial, we carry out the procedure described in [25], which extracts from b_{mn}, its dependence on a_{mn}, by writing it in the form

$$b_{mn} = DF(a_{00}) a_{mn} + c_{mn},$$

where c_{mn} depends only on lower order terms. That is, c_{mn} depends on a_{jk} where $0 \leq j \leq m$ and $0 \leq k \leq n$. Finally, recalling that $a_{00} = \mathbf{u}_0$, we rewrite Equation (28) as

$$\left[DF(\mathbf{u}_0) - (m\lambda_1 + n\lambda_2)\mathrm{Id}\right] a_{mn} = -c_{mn}. \tag{29}$$

The equations of (29) are called the *homological equations* for P, and we note that each these are linear equations for the Taylor coefficients of P with the right hand side depending only on lower order coefficients.

Remark 7 (The formal series is well defined). Since the eigenvalues have the form

$$\lambda_1 = \alpha + i\beta, \qquad \text{and} \qquad \lambda_2 = \mathrm{conj}(\lambda_1) = \alpha - i\beta,$$

we have that $m\lambda_1 + n\lambda_2$ is never an eigenvalue of $DF(\mathbf{u}_0)$ for any $(m, n) \in \mathbb{N}^2$. Therefore, the homological equations are uniquely solvable to any order for $m + n \geq 2$. Moreover, examination of Equation (29) shows that $a_{mn} = \mathrm{conj}(a_{nm})$ under the assumptions that $a_{00} \in \mathbb{R}^7$ and $\xi_1 = \mathrm{conj}(\xi_2)$.

This gives a direct proof, for the explicit case of the extended CRFBP, of the more general existence and uniqueness results alluded to in Section 3.1. That is, the homological equations are uniquely solvable (up to eigenvector scaling), hence we can compute the coefficients of P to any desired finite order. Moreover, the eigenvector scalings can be chosen so that these coefficients satisfy the complex conjugate condition described in Remark 3, so that P is $\mathbb{R}^7$-valued.

Now, suppose that $\{\bar{a}_{mn}\}_{0\leq m+n\leq N} \in \mathbb{C}^7$ is the result of solving for finitely many of these coefficients, then

$$P^N(z_1, z_2) = \sum_{0\leq m+n\leq N} \bar{a}_{mn} z_1^m z_2^n,$$

is our approximation of the (un)stable manifold. For the proof of the main result, the homological equations are solved using validated numerical methods similar to [25], resulting in interval enclosures for these Taylor coefficients, and rigorous bounds on the truncation error. The full implementation details for the finite computation and the validation of the truncation errors is the subject of the companion paper [61].

4.4 Formal integration of a material curve

Next, describe the formal integration of an analytic curve. Recalling the approach outlined in Section 3.2, let $\gamma\colon [-1,1] \to \mathbb{R}^7$ be a real analytic curve which we assume lies in the boundary of a local (un)stable manifold. Specifically, assume γ has a Taylor series expansion

$$\gamma(s) = \sum_{n=0}^{\infty} \gamma_n s^n \qquad \gamma_n \in \mathbb{R}^7.$$

We fix $\tau \in \mathbb{R}$ and look for a power series solution, $\Gamma\colon [-1,1]^2 \to \mathbb{R}^7$, of Equation (18) which we write as

$$\Gamma(s,t) = \sum_{m=0}^{\infty} \Gamma_m(s) t^m,$$

where

$$\Gamma_m(s) = \sum_{n=0}^{\infty} \Gamma_{mn} s^n.$$

Expanding the left hand side of Equation (18) as a power series leads to

$$\tau \frac{\partial}{\partial t}\Gamma(s,t) = \sum_{m=0}^{\infty} (m+1)\Gamma_{m+1}(s) t^m.$$

On the other hand, we assume an expansion of the right hand side of the form

$$F(\Gamma(s,t)) = \sum_{m=0}^{\infty} b_m(s) t^m,$$

where

$$b_m(s) = \sum_{n=0}^{\infty} b_{mn} s^n.$$

Matching like powers and solving for $\Gamma_{m+1}(s)$ leads to equations

$$\Gamma_{m+1}(s) = \frac{b_m(s)}{\tau(m+1)},$$

and we note further that $b_m(s)$ depends only on lower order terms. Hence, initializing with $\Gamma_0(s) = \gamma(s)$, these equations may be satisfied recursively to compute the Taylor expansion of $\Gamma(s,t)$ to any desired order. Again, since F is polynomial the details for making this computation rigorous are similar to those developed in [25]. As with the local parameterization, the method involves the interval enclosure of a finite approximation of the form

$$\Gamma^{MN}(s,t) = \sum_{m=0}^{M} \sum_{n=0}^{N} \Gamma_{mn} s^n t^m,$$

and rigorous estimates for the truncation error.

Remark 8 (Rescaling to control the coefficient growth). From a practical point of view, the most difficult part of growing the local stable/unstable manifolds is managing the rescaling and recentering of the manifold patches in an efficient and automated way. These technical details are managed using the techniques developed in [25].

4.5 Remarks on the tail validations for the formal series

Suppose that $g\colon D \to \mathbb{C}$ is an analytic function and g^N is a polynomial approximation of g. For example, in the context of the above discussion, g could be a scalar component of the local or global (un)stable manifold parameterization.

The goal of any validated numerical method is to obtain, with computer assistance, a mathematically rigorous error bound $r > 0$ of the form

$$\sup_{(z_1,z_2)\in D} \left| g^N(z_1,z_2) - g(z_1,z_2) \right| \leq r.$$

Note that if g is analytic on D, then

$$h(z_1,z_2) = g(z_1,z_2) - g^N(z_1,z_2),$$

defines an analytic function on D, and r provides a bound on the supremum norm of h.

It is then helpful to write

$$g(z_1,z_2) = g^N(z_1,z_2) + h(z_1,z_2),$$

so that

$$\sup_{(z_1,z_2)\in D} |g(z_1,z_2)| \leq \sup_{(z_1,z_2)\in D} \left| g^N(z_1,z_2) \right| + r,$$

gives a natural approach to bounding the truncation error. Note that in our case the polynomial part is computed with interval coefficients so that a rigorous bound for its supremum is easily obtained numerically. For example, considering derivatives we have that

$$\frac{\partial}{\partial z_1} g(z_1,z_2) = \frac{\partial}{\partial z_1} g^N(z_1,z_2) + \frac{\partial}{\partial z_1} h(z_1,z_2),$$

where the partial derivative of a polynomial is once again easy to compute numerically. Derivatives of the truncation error h are obtained on any smaller domain than D by using classical estimates or complex analysis. See for example the Cauchy Bounds of Lemma 2.9 of [27]. Of course these remarks generalize to other/higher order derivatives of g in the obvious way.

Implementation of the computer assisted error analysis used for the CRFBP is discussed in the companion paper [61]. Roughly speaking, the idea of the error analysis is to exploit that the unknown function solves a functional equation (invariance equation for the parameterization method in the case of P and the differential equation in the case of Γ). The functional equation is used in conjunction with the known polynomial approximation P^N or Γ^N to derive a fixed point problem for the truncation error $h(z_1, z_2)$ on an appropriate function space.

5 Computer assisted proof of a transverse homoclinic

In this section, we conclude the proof of Theorem 1.3. Specifically, we verify the hypotheses of Theorem 1.2 by explicitly computing a validated intersection of the stable and unstable manifolds, and then proving transversality for this intersection. Throughout this section we use the following notation. Recall that $||z||_\infty$ denotes the max norm on $\mathbb{C}^d$ as defined in Appendix A. For any $r \in \mathbb{R}^+$, let

$$B_r(z_0) = \{z \in \mathbb{C}^d : \ ||z - z_0||_\infty < r\}$$

denote the open ball of radius r, and let C_r^d denote the space of bounded analytic functions, $g : B_r(0) \to \mathbb{C}^d$, which we equip with the norm

$$||g||_r = \sup_{z \in B_r(0)} ||g(z)||_\infty .$$

5.1 Local manifolds

The local stable and unstable manifolds are each computed to order 7 using the methods discussed in Section 3.1. This yields a parameterization for $W^u_{\text{loc}}(\mathbf{x}_0)$ of the form

$$Q(z_1, z_2) = \sum_{0 \le m+n \le 7} q_{m,n} z_1^m z_2^n + h_Q(z_1, z_2),$$

where each $q_{m,n} \in \mathbb{IR}^7$ is an interval vector, and $h_Q \in C_1^2$ with a rigorous error bound

$$||h_Q||_1 \le r_Q = .5048 \times 10^{-16}.$$

Any arc segment transverse to the linear flow can be parameterized, and then rigorously lifted through the local unstable manifold parameterization to obtain a parameterized arc segment, $\gamma^u : [-1, 1] \to \mathbb{R}^7$, which is transverse to Φ and satisfies

$$\gamma^u([-1, 1]) \subseteq W^u_{\text{loc}}(\mathbf{x}_0),$$

For this validation, we lifted a piecewise linear closed curve transverse to the linear flow to obtain a collection of 20 boundary arcs

$$\gamma^u_*(s) = \sum_{n=0}^{15} a_n s^n + h^u_*(s),$$

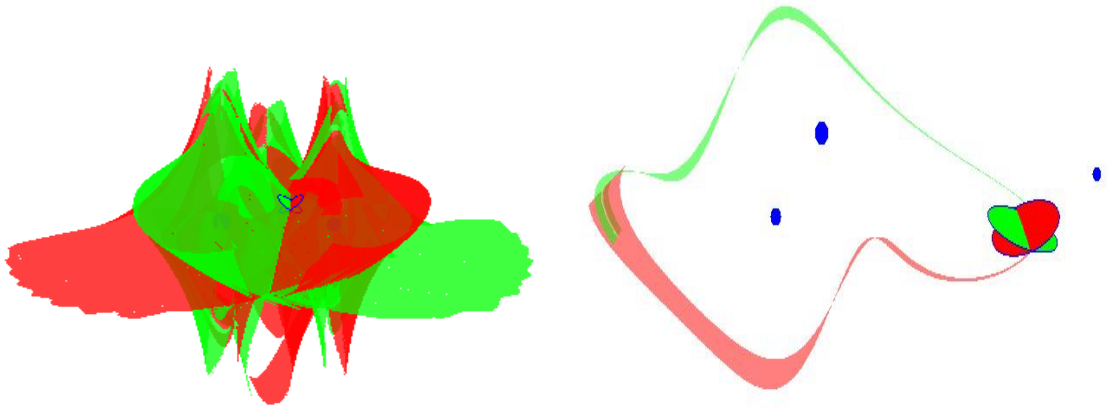

Figure 7: Projection of the (un)stable manifold atlases for the CRFBP on the $(x, y, \dot{y})$ coordinates. (Left) The image of thousands of polynomial chart maps obtained by advecting the boundaries of the local stable (green) and unstable (red) parameterizations. The local patches are the disks with blue boundaries in the center of the frame. (Right) A candidate intersection extracted from the atlases by checking the patches pairwise. The preimages under advection are shown all the way back to the local manifold boundaries. Note that each Figure illustrates three dimensional projections of four dimensional objects, and the apparent intersection of the manifolds in a straight line through the center of the local manifolds is of course, not truly an intersection. The actual local manifolds intersection only at the saddle-focus equilibrium point.

where $a_n \in \mathbb{IR}^7$, $h^u_* \in C^1_1$, and a rigorous bound, $||h^u_*||_1 \leq r^u = .2936 \times 10^{-13}$, which holds for all 20 unstable boundary arcs.

A similar parameterization is carried out for the stable manifold to obtain a collection of boundary arcs mapping into $W^s_{\rm loc}(\mathbf{x}_0)$ of the form

$$\gamma^s_*(s) = \sum_{n=0}^{15} b_n s^n + h^s_*(s)$$

with $||h^s_*||_1 \leq r^s = .3050 \times 10^{-13}$ for all 20 stable boundary arcs.

5.2 Growing an atlas

We obtain the global stable/unstable manifolds by advecting the initial boundary arcs using the formal series calculations discussed in Section 4, the computer assisted validation techniques of [61], and the automatic remeshing and rescaling algorithms developed in [25]. For example, advecting the boundaries of the stable/unstable manifolds for five time units forward/backward leads to the manifold atlases illustrated in the left frame of Figure 7. The stable atlas is comprised of $6,546$ and the unstable manifold comprised of $6,753$ polynomial chart maps. Each chart is computed to order 15 in the spatial direction and order 50 in time. The validated manifold patches have error bounds ranging from about 10^{-11} close to the parameterized local manifolds, to 10^{-4} near the end of the calculation.

Next, we search the results for homoclinic connection candidates, which are then post-processed using the computer assisted methods of proof discussed in Section 2.1. A candidate connection is illustrated in the right frame of Figure 7. The proof is discussed in more detail in the next section. For now we only remark that if the proof of the candidate connection fails then we can recover the "parent" charts of the candidates all the way back to the boundary of the invariant manifold and we can recompute to forward advection using increased accuracy. This is much cheaper than recomputing the entire atlas with increased accuracy.

5.3 Existence of a transverse intersection

After identifying a pair of charts with potential transverse intersection as discussed above, we use Lemma 1.4 to establish the existence of a true intersection point. Recall that the Lemma restates the existence of an intersection of the stable/unstable manifolds in terms of the solutions of a certain zero finding problem, defined in terms of the candidate charts. The next step is to run a non-rigorous numerical Newton method to refine the approximate intersections. This numerical calculation is carried out using the polynomial (truncated) part of the charts.

Specifically, given a pair of charts, Γ^u, Γ^s, which are candidates for an intersection of the stable/unstable manifolds, we run Newton's method (non-rigorously) to obtain parameters, $(\bar{s}, \bar{t}, \bar{\sigma}) \in \mathbb{R}^3$, such that $\Gamma^s(\bar{s}, \bar{t}) \approx \Gamma^u(\bar{\sigma}, 0)$. Now, we compute the a-posteriori estimates discussed in Theorem 2.1. If the estimates satisfy the theorem, then the a-posteriori validation succeeds and we check the condition described in Lemma 1.4 to conclude the existence of a true homoclinic in an explicit neighborhood of $\Gamma^u(\bar{s}, \bar{t})$. In fact the argument is very similar to the example proof discussed in Section **??**. Finally, we verify the hypothesis of Lemma 1.5 and conclude that the homoclinic is transverse.

Below, we explicitly describe the a-posteriori estimates obtained for a pair of charts lying in the intersection shown on the right of Figure 7. Recall that the stable chart may be decomposed as $\Gamma^s = P^N + P^\infty$ where P^N is a polynomial with $(M, N) = (15, 50)$ and $P^\infty \in C^2_1$. A similar decomposition for the unstable chart is given by $\Gamma^u = Q^N + Q^\infty$. We define

$$F(s, t, \sigma) = P(s, t) - Q(\sigma, 0) = F^N(s, t, \sigma) + F^\infty(s, t, \sigma),$$

and applying Newton iteration to F we find $(\bar{s}, \bar{t}, \bar{\sigma}) = (-.1421, -.0682, .0946) = \bar{x}$ satisfying $F^N(\bar{x}) \approx 0$. In other words, we take our approximate zero for F to be an approximate zero for the polynomial part of F. Now, we define $A^\dagger$ to be the matrix obtained by evaluating the formula $DF^N(\bar{x})$ using double precision floating point arithmetic (no interval enclosures), and let A be any numerical inverse of $A^\dagger$.

Next, we have a lemma which allows us to control derivatives of bounded analytic functions on $B_1(0) \subset \mathbb{C}^3$ by restricting to a smaller polydisc.

Lemma 5.1. Suppose $g \in C^3_1$ is a bounded analytic function defined on $B_1(0)$. Then for any $\nu > 0$, we have the bounds

$$||Dg||_{e^{-\nu}} \leq \frac{6\pi}{\nu} ||g||_1$$
$$\left|\left|D^2 g\right|\right|_{e^{-\nu}} \leq \frac{36\pi^2}{\nu^2} ||g||_1$$

A proof of this lemma for arbitrary dimension can be found in [27]. With this in hand, set (somewhat arbitrarily) $r_* = 7 \times 10^{-3}$ and set

$$\nu = -\ln(||\bar{x}||_\infty + r_*) = 1.9028,$$

and note that $B_{r_*}(\bar{x}) \subseteq B_{e^{-\nu}}(0)$. Now, we are prepared to compute the a-posteriori estimates required for Theorem 2.1. All computations below are carried out using interval arithmetic with floating point numbers regarded as degenerate intervals of the form $[x, x] \in \mathbb{IR}$.

5.3.1 Y_0

We note that we have an error bound for F^∞ given by $||F^\infty||_1 \leq ||P^\infty||_1 + ||Q^\infty||_1$ which leads to the enclosure

$$F(\bar{x}) \in [F^N(\bar{x}) - ||F^\infty||_1, F^N(\bar{x}) + ||F^\infty||_1].$$

From this estimate, we compute the enclosure $||A \cdot F(\bar{x})||_\infty \in [0, .0054]$ and we take $Y_0 = .0054$.

5.3.2 Z_0

Let I denote the 3×3 identify matrix, then we explicitly compute

$$\left|\left|I - AA^\dagger\right|\right|_\infty \in [0, .1349 \times 10^{-14}].$$

Hence, we take $Z_0 = .1349 \times 10^{-14}$.

5.3.3 Z_1

We decompose $DF(\bar{x}) = DF^N(\bar{x}) + DF^\infty(\bar{x})$ and apply Lemma 5.1 to obtain

$$||DF^\infty||_{e^{-\nu}} \leq \frac{6\pi}{\nu} ||F^\infty||_1 \leq 4.3739 \times 10^{-4}.$$

It follows that

$$\sup_{y \in B_{r_*}(\bar{x})} ||DF^\infty(y)||_\infty \leq ||DF^\infty||_{e^{-\nu}} \leq 4.2815 \times 10^{-4}.$$

Combining this result with an interval computation on the finite part we obtain

$$DF(\bar{x}) \in [DF^N(\bar{x}) - 4.2815 \times 10^{-4}, DF^N(\bar{x}) + 4.2815 \times 10^{-4}],$$

and we use this interval enclosure to compute

$$\left|\left|A(A^\dagger - DF(\bar{x})\right|\right|_\infty \in [0, .1538].$$

Hence, we set $Z_1 = .1538$.

5.3.4 Z_2

Similarly, we decompose $DF(\bar{x}) = DF^N(\bar{x}) + DF^\infty(\bar{x})$ and apply the second part of Lemma 5.1 to obtain the enclosure

$$\left|\left|D^2F^\infty\right|\right|_{e^{-\nu}} \leq \frac{36\pi^2}{\nu^2}\left|\left|F^\infty\right|\right|_1 \leq .0043,$$

which yields the bound

$$\sup_{y\in B_{r_*}(\bar{x})}\left|\left|D^2F^\infty(y)\right|\right|_\infty \leq \left|\left|D^2F^\infty\right|\right|_{e^{-\nu}} \leq .0043.$$

Turning to the finite part, we apply the formula given in Appendix B which yields

$$\begin{aligned}
\sup_{y\in B_{r_*}(\bar{x})}\left|\left|D^2F^N(y)\right|\right|_\infty &= \sup_{y\in B_{r_*}(\bar{x})}\max_{1\leq i\leq 3}\sum_{j=1}^{3}\sum_{k=1}^{3}\left|\partial_j\partial_k F_i^N(y)\right| \\
&\leq \max_{1\leq i\leq 3}\sum_{j=1}^{3}\sum_{k=1}^{3}\sup_{y\in B_{r_*}}\left|\partial_j\partial_k F_i^N(y)\right| \\
&= \max_{1\leq i\leq 3}\sum_{j=1}^{3}\sum_{k=1}^{3}\left|\left|\partial_j\partial_k F_i^N\right|\right|_{B_{r_*}(\bar{x})}.
\end{aligned}$$

For each $i = 1, 2, 3$, the terms in the sum are computed with interval arithmetic and taking the max yields

$$\sup_{y\in B_{r_*}(\bar{x})}\left|\left|D^2F^N(y)\right|\right|_Q \leq .0151.$$

Taking these bounds together, we obtain the estimate

$$\begin{aligned}
\sup_{y\in B_{r_*}(\bar{x})}\left|\left|D^2F(y)\right|\right|_\infty &\leq \sup_{y\in B_{r_*}(\bar{x})}\left|\left|D^2F^N(y)\right|\right|_\infty + \sup_{y\in B_{r_*}(\bar{x})}\left|\left|D^2F^\infty(y)\right|\right|_\infty \\
&\leq .0043 + .0151 = .0194.
\end{aligned}$$

Finally, a rigorous computation yields the bound $||A||_\infty \leq 84.6195$, leading to the enclosure

$$||A|| \cdot \sup_{y\in B_{r_*}}\left|\left|D^2F(y)\right|\right| \in [2.3284, 2.3414],$$

and thus we set $Z_2 = 2.3414$.

Finally, we verify that Theorem 2.1 holds by computing the radii polynomial,

$$p(r) = Z_2r^2 - (1 - Z_0 - Z_1)r + Y_0 = 2.3414r^2 - .8462r + .0053$$

which has roots given by $(r_-, r_+) = (.0064, .3550)$. Noting that $r_- < r_*$, we conclude that $p(r) < 0$ for all $r \in [.0064, .007]$. Hence, setting $r = r_- = .0064$, it follows from Theorem 2.1 that there exists a unique $\hat{x} = (\hat{s}, \hat{t}, \hat{\sigma}) \in B_r(\bar{x})$ such that $F(\hat{x}) = 0$.

Next, we verify Lemma 1.4 holds. We consider the rectangle, $B_r(\bar{s}, \bar{t}) \in \mathbb{IR}^2$, and the interval $B_r(\bar{\sigma}) \in \mathbb{IR}$, so that via interval arithmetic we compute the enclosures

$$\begin{aligned}
\Gamma_4^u(B_r(\bar{s}, \bar{t})) &\in [-.1629, -.1619], \\
\Gamma_4^s(B_r(\bar{\sigma}), 0) &\in [-.1633, -0.1615],
\end{aligned}$$

and we conclude that $\Gamma_4^u(\hat{s},\hat{t})$ has the same sign as $\Gamma_4^s(\hat{\sigma},0)$. Thus, by Lemma 1.4, the orbit of $\Gamma^u(\hat{s},\hat{t})$ is a homoclinic for the saddle focus $\mathbf{x}_0$.

Finally, the transversality is verified using Lemma 1.5. First note that invertibility of $DF(\hat{x})$ is a conclusion of Theorem 2.1. Then, to verify the hypotheses of Lemma 1.5 it suffices to check that $\nabla E(\Gamma^u(\hat{s},\hat{t})) \neq 0$ which holds if any coordinate is nonzero. In particular, we compute the 2^{nd} coordinate rigorously

$$\pi_2 \circ \nabla E = \partial_2 E = \Gamma_2^u(B_r(\bar{x})) \in [-0.0747, -.0618],$$

and note that $0 \notin [-0.0747, -.0618]$. Thus, we conclude that $\Gamma_2^u(\hat{s},\hat{t}) \neq 0$ and therefore, $\nabla E(\Gamma^u(\hat{s},\hat{t})) \neq 0$, proving that this homoclinic is transverse. Combining these results, we have proved Theorem 1.3 , namely that the orbit of $\Gamma^u(\hat{s},\hat{t})$ is homoclinic to $\mathbf{x}_0$ and transverse in the energy section.

5.4 Bounding transport times

The global parameterization of the (un)stable manifolds for the saddle-focus at $\mathbf{x}_0$ is the backbone of our proof. Of course, there are other methods for validating homoclinic orbits in the literature which may allow one to prove existence of a transverse homoclinic with significantly less effort or more final accuracy. The real value in computing a global atlas for the stable and unstable manifolds is that this method can also rule out connections. In other words, our interest in this paper is not only to prove that the CRFBP is chaotic, but also, to show that our method of verifying the Strömgren hypothesis also provides rigorous bounds on the transport times for *all* homoclinic connections.

To make this more precise, suppose Γ^s, Γ^u are any pair of analytic charts for the stable/unstable manifolds of $\mathbf{x}_0$ respectively. Following our scheme outlined in Section 3.2, we obtain Γ^s in the form

$$\Gamma^s(s,t) = \sum_{m=0}^{M}\sum_{n=0}^{N} b_{mn} s^n t^m + h^s(s,t)$$

where each $a_{mn} \in \mathbb{IR}$ and h^u is analytic and satisfying $||h^u||_1 \leq r^u$ for $r^u \in (0,\infty)$. Similarly, we obtain

$$\Gamma^u(s,t) = \sum_{m=0}^{M}\sum_{n=0}^{N} a_{mn} s^n t^m + h^u(s,t)$$

where each $b_{mn} \in \mathbb{IR}$ and h^s is analytic and satisfying $||h^s||_1 \leq r^s$ for $r^s \in (0,\infty)$. Now, we define $F : [-1,1]^4 \to \mathbb{IR}$ given by

$$F(s_1,t_1,s_2,t_2) = \Gamma^s(s_1,t_1) - \Gamma^u(s_2,t_2).$$

Evidently, if F has no roots on $[-1,1]^4$, then Γ^s and Γ^u are non-intersecting charts. The rigorous verification of this follows by evaluating the finite part of F with interval arithmetic and padding by the interval $[-(r^u+r^s),(r^u+r^s)]$. We carried out this computation pairwise for stable and unstable charts contained in the atlases shown on the left side of Figure 7 until a connection could not be ruled out. In fact, the first instance in which this procedure failed occurs for a pair of charts which do contain a transverse homoclinic connection. By rigorously ruling out all pairwise charts with shorter (combined) integration time, we obtain the following result.

Theorem 5.2. Let $W^s_{\mathrm{loc}}(\mathbf{x}_0)$, $W^u_{\mathrm{loc}}(\mathbf{x}_0)$ be the validated local stable/unstable manifolds computed to order 7 as described in Section 5.1. Suppose γ is a homoclinic connection for $\mathbf{x}_0$ which exits $W^u_{\mathrm{loc}}(\mathbf{x}_0)$ at time t_0, and intersects $W^s_{\mathrm{loc}}(\mathbf{x}_0)$ at time $t_f < t_0 + 4.1437$ time units. Then, for some $t_0 \le t \le t_f$, we have $\sqrt{\gamma_2(t)^2 + \gamma_4(t)^2} > 1.7$. In other words, for every homoclinic orbit for $\mathbf{x}_0$ whose *speed* along the orbit obeys the bound $\sqrt{\dot{x}^2 + \dot{y}^2} < 1.7$, the connection time for the orbit is bounded below by 4.1437 time units.

Acknowledgments

The authors wish to thank Robert Devaney, Jan Bouwe van den Berg, J.P. Lessard, and Jaime Burgos for helpful conversations. Both authors were partially supported by NSF grant DMS-1700154 and by the Alfred P. Sloan Foundation grant G-2016-7320 during the work on this research.

A Norms in $\mathbb{R}^d \backslash \mathbb{C}^d$

Let $V = \mathbb{R}^d$ or $V = \mathbb{C}^d$, and write $\mathbf{v} = (v_1, \ldots, v_d)$ to denote an element of V. Endow V with the max-norm

$$\|v\|_\infty := \max_{1 \le j \le d} |v_j|, \tag{30}$$

where $|\cdot|$ is the real or complex absolute value as appropriate.

Similarly, suppose A is a $d \times d$ matrix over $\mathbb{R}$ or $\mathbb{C}$ and let $\{a_{ij}\}_{1 \le i,j \le d}$ denote the entries of A. Then the matrix norm

$$\|A\|_M := \max_{1 \le i \le d} \sum_{j=1}^{d} |a_{ij}|,$$

is the operator norm on the space of linear operators from V to V induced by the max-norm of Equation (30), which satisfies the useful bound

$$\|Av\| \le \|A\|_M \|v\| \qquad v \in V. \tag{31}$$

Finally, we consider a $d \times d \times d$ *matroid* B and let $\{b_{ijk}\}_{1 \le i,j,k \le d}$ denote the entries of B. Then B defines a V-valued bi-linear mapping on $V \times V$ with action given by the formula

$$B(u,v)_i = \sum_{j=1}^{d} \sum_{k=1}^{d} b_{ijk} u_j v_k, \qquad\qquad u, v \in V,$$

where $B(u,v)_i$, denotes the i-th component of $B(u,v) \in V$. Similarly, the max-norm on V induces the *matroid norm*

$$\|B\|_Q := \max_{1 \le i \le d} \sum_{j=1}^{d} \sum_{k=1}^{d} |b_{ijk}|,$$

which satisfies the bound

$$\|B(u,v)\| \le \|B\|_Q \, \|u\| \, \|v\| \qquad u, v \in V. \tag{32}$$

B Bounds on first and second derivatives

Suppose that $U \subset V$ is an open set, $g\colon U \to V$ is a smooth map, and $\mathbf{v} \in V$. We write $g = (g_1, \ldots, g_d)$ to denote the component maps. The derivative of g at $\mathbf{v}$ is the linear operator represented by the $d \times d$ *Jacobian matrix*, $A = Dg(\mathbf{v})$, with entries given by

$$a_{ij} = \partial_j f_i(\mathbf{v}), \qquad 1 \le i, j \le d,$$

and from Appendix A, we have the explicit expression for its operator norm

$$\|Dg(\mathbf{v})\|_M = \max_{1 \le i \le d} \sum_{j=1}^{d} |\partial_j f_i(\mathbf{v})|\,. \tag{33}$$

Similarly, the second derivative of g at $\mathbf{v}$ is a bi-linear mapping, $B = D^2 f(\mathbf{v})$, with entries given by

$$b_{ijk} = \partial^2_{jk} f_i(\mathbf{v}), \qquad 1 \le i, j, k \le d,$$

and its operator norm is given explicitly by

$$\|D^2 g(\mathbf{v})\|_Q = \max_{1 \le i \le d} \sum_{j=1}^{d} \sum_{k=1}^{d} \left|\partial^2_{jk} f_i(\mathbf{u})\right|. \tag{34}$$

We have the following estimate, whose proof is a calculation we leave to the interested reader.

Lemma B.1. *Fix $r_* > 0$, $\overline{\mathbf{u}} \in U \subset V$, and suppose that $\overline{B_{r_*}(\overline{\mathbf{u}})} \subset U$. Then for any $\mathbf{u}, \mathbf{v} \in \overline{B_{r_*}(\overline{\mathbf{u}})}$, we have the bound*

$$\|Dg(\mathbf{u}) - Dg(\mathbf{v})\|_M \le \sup_{\mathbf{w} \in \overline{B_{r_*}(\overline{\mathbf{u}})}} \left\|D^2 g(\mathbf{w})\right\|_Q \|u - v\|. \tag{35}$$

C Some explicit formulas for the CRFBP

Primary Coordinates

Define the constant

$$K := m_2(m_3 - m_2) + m_1(m_2 + 2m_3),$$

and denote the coordinates of the 3 primaries (in configuration space) as

$$p_1 = (x_1, y_1), \qquad p_2 = (x_2, y_2), \qquad \text{and} \qquad p_3 = (x_3, y_3).$$

These coordinates are given explicitly in terms of K by

$$x_1 = \frac{-|K|\sqrt{m_2^2 + m_2 m_3 + m_3^2}}{K} \qquad y_1 = 0$$

$$x_2 = \frac{|K|\left[(m_2 - m_3)m_3 + m_1(2m_2 + m_3)\right]}{2K\sqrt{m_2^2 + m_2 m_3 + m_3^2}} \qquad y_2 = \frac{-\sqrt{3}m_3}{2m_2^{3/2}}\sqrt{\frac{m_2^3}{m_2^2 + m_2 m_3 + m_3^2}}$$

$$x_3 = \frac{|K|}{2\sqrt{m_2^2 + m_2 m_3 + m_3^2}} \qquad y_3 = \frac{\sqrt{3}}{2\sqrt{m_2}}\sqrt{\frac{m_2^3}{m_2^2 + m_2 m_3 + m_3^2}}.$$

Eigenvalues/Eigenvectors at a saddle-focus

By inspecting Equation (3), we see that if $\mathbf{x}_0 = (x, \dot{x}, y, \dot{y})$ is an equilibrium for f, then $\dot{x} = \dot{y} = 0$. A direct computation shows that the Jacobian matrix is given by

$$Df(\mathbf{x}_0) = \begin{pmatrix} 0 & 1 & 0 & 0 \\ \Omega_{xx}(\mathbf{x}_0) & 0 & \Omega_{xy}(\mathbf{x}_0) & 2 \\ 0 & 0 & 0 & 1 \\ \Omega_{yx}(\mathbf{x}_0) & -2 & \Omega_{yy}(\mathbf{x}_0) & 0 \end{pmatrix}$$

Suppressing the evaluation at $(\mathbf{x}_0)$, and using the fact that $\Omega_{xy} = \Omega_{yx}$, we have the formula for the eigenvalues of $Df(\mathbf{x}_0)$ given by

$$\lambda_{1,2,3,4} = \pm\sqrt{\frac{-(4 - \Omega_{xx} - \Omega_{yy}) \pm \sqrt{(4 - \Omega_{xx} - \Omega_{yy})^2 - 4(\Omega_{xx}\Omega_{yy} - \Omega_{xy}^2)}}{2}}. \tag{36}$$

The following Lemma, whose proof is again a straightforward calculation, provides the associated eigenvectors.

Lemma C.1. *Let $\lambda \in \mathbb{C}$ be a nonzero eigenvalue for $Df(\mathbf{x}_0)$, and define the vectors*

$$\mathbf{v}_1 = \begin{pmatrix} 1 \\ \lambda \\ 0 \\ 0 \end{pmatrix}, \qquad \textit{and} \qquad \mathbf{v}_2 = \begin{pmatrix} 0 \\ 0 \\ 1 \\ \lambda \end{pmatrix}.$$

Fix $s \in \mathbb{C}$ with $s \neq 0$, and define

$$r = -s\frac{\Omega_{xy} + 2\lambda}{\Omega_{xx} - \lambda^2}, \qquad \textit{and} \qquad \xi = r\mathbf{v}_1 + s\mathbf{v}_2,$$

then ξ is an eigenvector of $Df(\mathbf{x}_0)$ associated with the eigenvalue λ.

D Further discussion of Theorem 4.1

In this section, we sketch a proof of Theorem 4.1. In particular, we give an overview of the computations for the three main claims in the Theorem: orbit correspondence, linear stability, and invariant Manifolds.

Orbit correspondence

We begin by showing that the map, R, defined in Equation (21), lifts every trajectory of Ψ, to a corresponding trajectory of Φ. To see this, let $\mathbf{x} \in U$, and suppose that $\gamma\colon (-T, T) \to \mathbb{C}^4$ satisfies the initial value problem $\gamma' = f(\gamma)$ with $\gamma(0) = \mathbf{x}$. Then, a trivial computation shows that $\Gamma\colon (-T, T) \to \mathbb{C}^7$ defined by

$$\Gamma(t) := R(\gamma(t)),$$

satisfies the initial value problem, $\Gamma' = F(\Gamma)$ with $\Gamma(0) = R(\mathbf{x})$.

Moreover, we have the following partial converse. Suppose $\Gamma\colon (-T,T) \to \mathbb{C}^7$ parameterizes a trajectory segment of Φ, and assume in addition that $\pi \circ \Gamma(-T,T) \subset U$, then the converse holds since

$$\gamma(t) = \pi \circ \Gamma(t),$$

satisfies the initial value problem $\gamma' = f(\gamma)$, with initial data $\gamma(0) = \pi(\Gamma(0))$.

Taken together, these computations justify the orbit correspondence claimed in Theorem 4.1. Furthermore, all equilibrium solutions for f lie in U and therefore, give rise to an equilibrium for F which lies in $\mathcal{S}$ for all time.

Linear stability

Next, recall that $\mathbf{x}_0$ is a saddle-focus equilibrium for f and let $\mathbf{u}_0 = R(\mathbf{x}_0)$ denote the associated equilibrium for F. We claim that $Df(\mathbf{x}_0)$ has a "similar" linear stability to $DF(\mathbf{u}_0)$ in the sense that the two-dimensional stable/unstable linear subspaces attached to $\mathbf{x}_0$, are pushed forward by $DR(\mathbf{x}_0)$ to a corresponding two-dimensional stable/unstable linear subspace attached to $\mathbf{u}_0$.

This follows by first differentiating Equation (24) with respect to $\mathbf{x}$ to obtain

$$DF(R(\mathbf{x}))DR(\mathbf{x}) = D^2R(\mathbf{x})f(\mathbf{x}) + DR(\mathbf{x})Df(\mathbf{x}). \tag{37}$$

Here $D^2R(\mathbf{x})$ is a bilinear mapping, and the meaning of the notation, $D^2R(\mathbf{x})f(\mathbf{x})$, is that one of the two arguments has $f(\mathbf{x})$ fixed. Hence, the resulting expression, $D^2R(\mathbf{x})f(\mathbf{x})$, defines a linear mapping like everything else in the expression. Evaluation of Equation (37) at $\mathbf{x}_0$ leads to the identity

$$DF(\mathbf{u}_0)DR(\mathbf{x}_0) = DR(\mathbf{x}_0)Df(\mathbf{x}_0), \tag{38}$$

where we have used the fact that $\mathbf{x}_0$ is an equilibrium for f, and the identity, $\mathbf{u}_0 = R(\mathbf{x}_0)$.

A straight-forward analysis of Equation (38) shows that every distinct eigenvalue of $Df(\mathbf{x}_0)$ also appears as an eigenvalue of $DF(\mathbf{u}_0)$. Recalling our assumption that $\mathbf{x}_0$ is a saddle-focus, this implies that $DF(\mathbf{u}_0)$ has two pairs of complex conjugate eigenvalues. Moreover, the explicit formula for the eigenvectors of $DF(\mathbf{u}_0)$ given in Theorem 4.1 is again an immediate consequence of Equation (38).

On the other hand, $DF(\mathbf{u}_0)$ can be computed explicitly using the formulas for F and R given in Section 4.1, and after row-reducing this matrix, it can be shown that $\ker(DF(\mathbf{u}_0))$ has dimension at least 3. Since the above computation yielded 4 distinct, non-zero eigenvalues for the 7-by-7 matrix, $DF(\mathbf{u}_0)$, we conclude that the remaining 3 eigenvalues for $DF(\mathbf{u}_0)$ are zero which completes the proof of the claim.

Invariant manifolds

We consider the stable manifolds with the result for unstable manifolds following as usual. Let $\lambda^s_{1,2}$ and $\xi^s_{1,2}$ denote the stable eigenvalues/eigenvectors as in Theorem 4.1. From the result on linear stability, these are also stable eigenvalues for $DF(\mathbf{u}_0)$ with their corresponding eigenvectors given by

$$\mathbf{v}^s_{1,2} := R(\mathbf{x}_0)\xi^s_{1,2}.$$

Now, we begin with the following Lemma.

Lemma D.1. *Suppose that $P\colon D \to \mathbb{C}^7$ solves the invariance equation (13) subject to the first order constraints, $P(0) = \mathbf{u}_0$, $\partial_1 P(0) = \mathbf{v}_1^s$, and $\partial_2 P(0) = \mathbf{v}_2^s$, and assume that $\pi \circ P(D) \subset U$, then*

$$P(D) \subset \mathcal{S}.$$

Proof. Let $\mathbf{z} = (z_1, z_2) \in D$, and define the curve $\Gamma\colon [0,\infty) \to \mathbf{C}^7$ by

$$\Gamma(t) := P(e^{\lambda_1 t} z_1, e^{\lambda_2 t} z_2).$$

By Lemma 3.1, we have that Γ satisfies the initial value problem $\Gamma' = F(\Gamma)$ with $\Gamma(0) = P(\mathbf{z})$, and

$$\lim_{t\to\infty} \Gamma(t) = \mathbf{u}_0.$$

Since $\pi \circ P(D) \subset U$, it follows that $\Gamma(0) \in \mathcal{S}$. In fact, for all $t \geq 0$ we have $\Gamma(t) \in P(D) \subset \mathcal{S}$ implying that $\Gamma([0,\infty)) \subset \mathcal{S}$. Since $\mathbf{z} \in D$ was arbitrary we have the result. □

Now, assume P is as in the previous lemma, and define $p = \pi \circ P\colon D \to \mathbb{C}^4$. To show that p parameterizes a stable manifold for f, we need to show that p solves the invariance equation (13) for the CRFBP with the appropriate first order constraints. To see this, let $\mathbf{z} \in D$, so that by applying Lemma D.1 we have

$$P(\mathbf{z}) \in \mathcal{S} = R(U).$$

Recalling the identity of Equation (22), it follows that

$$P(\mathbf{z}) = R(\pi P(\mathbf{z})) = R(p(\mathbf{z})),$$

and combining with Equation 23 we obtain

$$\pi F(P(\mathbf{z})) = \pi F(R(p(\mathbf{z}))) = f(p(\mathbf{z})).$$

Taken together, and recalling that P satisfies Equation (13) for F, a simple computation shows that

$$\lambda_1 z_1 \frac{\partial}{\partial z_1} p(z_1, z_2) + \lambda_2 z_2 \frac{\partial}{\partial z_2} p(z_1, z_2) = f(p(z_1, z_2)).$$

Since this holds for all $\mathbf{z} \in D$, it follows that p satisfies Equation (13) on D.

Finally, it remains only to check that the first order constraints are satisfied. For this, we note that the stable eigenvectors for $Df(\mathbf{x}_0)$ and $DF(\mathbf{u}_0)$ satisfy $\pi \mathbf{v}_{1,2}^s = \xi_{1,2}^s$. This identity leads to the following computations for the first order data for p:

$$p(0) = \pi P(0) = \pi \mathbf{u}_0 = \mathbf{x_0} \tag{39}$$

$$\frac{\partial}{\partial z_1} p(0) = \pi \frac{\partial}{\partial z_1} P(0) = \pi \mathbf{v}_1^s = \xi_1^s \tag{40}$$

$$\frac{\partial}{\partial z_2} p(0) = \pi \frac{\partial}{\partial z_2} P(0) = \pi \mathbf{v}_2^s = \xi_2^s \tag{41}$$

and we conclude by Lemma 3.1 that p parameterizes a local stable manifold for $\mathbf{x}_0$.

References

[1] G. H. Darwin. Periodic Orbits. *Acta Math.*, 21(1):99–242, 1897.

[2] F.R. Moulton, D. Buchanan, T Buck, F.L. Griffin, W.R. Longley, and W.D. MacMillan. *Periodic Orbits.* Number Publication No. 161. Carnegie Institution of Washington, 1920.

[3] E. Strömgren. Connaissance actuelle des orbites dans le probleme des trois corps. *Bull. Astron.*, 9:87–130, 1934.

[4] Roberto Castelli and Jean-Philippe Lessard. Rigorous Numerics in Floquet Theory: Computing Stable and Unstable Bundles of Periodic Orbits. *SIAM J. Appl. Dyn. Syst.*, 12(1):204–245, 2013.

[5] G. Shearing. PhD thesis, University of Manchester, 1960.

[6] James H. Bartlett. The restricted problem of three bodies. *Mat.-Fys. Skr. Danske Vid. Selsk.*, 2(7):48 pp. (1964), 1964.

[7] J. H. Bartlett and C. A. Wagner. The restricted problem of three bodies. II. *Mat.-Fys. Skr. Danske Vid. Selsk.*, 3(1):53 pp. (1965), 1965.

[8] M. Hénon. Exploration numérique du probléme restreint. *Ann. Astrophys.*, 28(499), 1965.

[9] J.M.A. Danby. Orbits in the copenhagen problem asymptotic at l_4, and their genealogy. *The Astronomical Journal*, 72(2):198 –201, 1967.

[10] V. Szebehely and Flandern T.V. A family of retegrade orbits around the triangular equilibrium points. *The Astronomical Journal*, 72(3):373–379, 1967.

[11] V. Szebehely and P. Nacozy. A class of e. strömgren's direct orbits in the restricted problem. *The Astronomical Journal*, 77(2):184–190, 1967.

[12] Jacques Henrard. Proof of a conjecture of E. Strömgren. *Celestial Mech.*, 7:449–457, 1973.

[13] Ralph H. Abraham. Chaostrophes, intermittency, and noise. In *Chaos, fractals, and dynamics (Guelph, Ont., 1981/1983)*, volume 98 of *Lecture Notes in Pure and Appl. Math.*, pages 3–22. Dekker, New York, 1985.

[14] Robert L. Devaney. Blue sky catastrophes in reversible and Hamiltonian systems. *Indiana Univ. Math. J.*, 26(2):247–263, 1977.

[15] L. M. Lerman. Behavior of a Hamiltonian system in a neighborhood of a transversal homoclinic saddle-focus trajectory. *Uspekhi Mat. Nauk*, 44(2(266)):233–234, 1989.

[16] Leonid Pavlovich Shilnikov, Andrey L. Shilnikov, and Dmitry V. Turaev. Showcase of blue sky catastrophes. *Internat. J. Bifur. Chaos Appl. Sci. Engrg.*, 24(8):1440003, 10, 2014.

[17] Antonis D. Pinotsis. Infinite Feigenbaum sequences and spirals in the vicinity of the Lagrangian periodic solutions. *Celestial Mech. Dynam. Astronom.*, 108(2):187–202, 2010. With supplementary material available online.

[18] B. Sicardy. Stability of the triangular Lagrange points beyond Gascheau's value. *Celestial Mech. Dynam. Astronom.*, 107(1-2):145–155, 2010.

[19] Robert L. Devaney. Homoclinic orbits in Hamiltonian systems. *J. Differential Equations*, 21(2):431–438, 1976.

[20] L. P. Silnikov. Existence of a countable set of periodic motions in a four-dimensional space in an extended neighborhood of a saddle-focus. *Dokl. Akad. Nauk SSSR*, 172:54–57, 1967.

[21] L. P. Silnikov. On the question of the structure of an extended neighborhood of a structurally stable state of equilibrium of saddle-focus type. *Mat. Sb. (N.S.)*, 81 (123):92–103, 1970.

[22] L. M. Lerman. Complex dynamics and bifurcations in a Hamiltonian system having a transversal homoclinic orbit to a saddle focus. *Chaos*, 1(2):174–180, 1991.

[23] S. Smale. Differentiable dynamical systems. *Bull. Amer. Math. Soc.*, 73:747–817, 1967.

[24] J. D. Mireles James. Validated numerics for equilibriua of analytic vector fields: invariant manifolds and connecting orbits. *(To appear in AMS lecture notes - winter short course series)*, pages 1–55, 2017.

[25] Shane Kepley, William D. Kalies, and J. D. Mireles James. Analytic continuation of local (un)stable manifolds with rigorous computer assisted error bounds. *(Submitted)*, pages 1–41, 2017.

[26] Jean-Philippe Lessard, Jason D. Mireles James, and Christian Reinhardt. Computer assisted proof of transverse saddle-to-saddle connecting orbits for first order vector fields. *J. Dynam. Differential Equations*, 26(2):267–313, 2014.

[27] J. D. Mireles James and Konstantin Mischaikow. Rigorous a-posteriori computation of (un)stable manifolds and connecting orbits for analytic maps. *SIAM J. Appl. Dyn. Syst.*, 12(2):957–1006, 2013.

[28] Eduardo S. G. Leandro. On the central configurations of the planar restricted four-body problem. *J. Differential Equations*, 226(1):323–351, 2006.

[29] Jean F. Barros and Eduardo S. G. Leandro. The set of degenerate central configurations in the planar restricted four-body problem. *SIAM J. Math. Anal.*, 43(2):634–661, 2011.

[30] Jean F. Barros and Eduardo S. G. Leandro. Bifurcations and enumeration of classes of relative equilibria in the planar restricted four-body problem. *SIAM J. Math. Anal.*, 46(2):1185–1203, 2014.

[31] Gianni Arioli. Periodic orbits, symbolic dynamics and topological entropy for the restricted 3-body problem. *Comm. Math. Phys.*, 231(1):1–24, 2002.

[32] Gianni Arioli. Branches of periodic orbits for the planar restricted 3-body problem. *Discrete Contin. Dyn. Syst.*, 11(4):745–755, 2004.

[33] Daniel Wilczak and Piotr Zgliczynski. Heteroclinic connections between periodic orbits in planar restricted circular three-body problem—a computer assisted proof. *Comm. Math. Phys.*, 234(1):37–75, 2003.

[34] Maciej J. Capiński and Piotr Zgliczyński. Transition tori in the planar restricted elliptic three-body problem. *Nonlinearity*, 24(5):1395–1432, 2011.

[35] Gianni Arioli, Vivina Barutello, and Susanna Terracini. A new branch of Mountain Pass solutions for the choreographical 3-body problem. *Comm. Math. Phys.*, 268(2):439–463, 2006.

[36] Alessandra Celletti and Luigi Chierchia. A computer-assisted approach to small-divisors problems arising in Hamiltonian mechanics. In *Computer aided proofs in analysis (Cincinnati, OH, 1989)*, volume 28 of *IMA Vol. Math. Appl.*, pages 43–51. Springer, New York, 1991.

[37] Maciej J. Capiński. Computer assisted existence proofs of Lyapunov orbits at L_2 and transversal intersections of invariant manifolds in the Jupiter-Sun PCR3BP. *SIAM J. Appl. Dyn. Syst.*, 11(4):1723–1753, 2012.

[38] Maciej Capiński and Pablo Roldán. Existence of a center manifold in a practical domain around L_1 in the restricted three body problem. *SIAM J. Appl. Dyn. Syst.*, 11(1):285–318, 2011.

[39] Maciej J. Capiński and Anna Wasieczko-Zajac. Geometric proof of strong stable/unstable manifolds with application to the restricted three body problem. *Topol. Methods Nonlinear Anal.*, 46(1):363–399, 2015.

[40] Maciej J. Capiński, Marian Gidea, and Rafael de la Llave. Arnold diffusion in the planar elliptic restricted three-body problem: mechanism and numerical verification. *Nonlinearity*, 30(1):329–360, 2017.

[41] Jean-Philippe Lessard, J. D. Mireles James, and Julian Ransford. Automatic differentiation for Fourier series and the radii polynomial approach. *(To Appear in Physica D)*.

[42] Tomasz Kapela and Carles Simó. Computer assisted proofs for nonsymmetric planar choreographies and for stability of the Eight. *Nonlinearity*, 20(5):1241–1255, 2007.

[43] Tomasz Kapela. N-body choreographies with a reflectional symmetry—computer assisted existence proofs. In *EQUADIFF 2003*, pages 999–1004. World Sci. Publ., Hackensack, NJ, 2005.

[44] Tomasz Kapela and Carles Simó. Rigorous KAM results around arbitrary periodic orbits for Hamiltonian systems. *Nonlinearity*, 30(3):965–986, 2017.

[45] Tomasz Kapela and Piotr Zgliczyński. The existence of simple choreographies for the N-body problem—a computer-assisted proof. *Nonlinearity*, 16(6):1899–1918, 2003.

[46] Jaime Burgos-Garcí a and Joaquí n Delgado. On the "blue sky catastrophe" termination in the restricted four-body problem. *Celestial Mech. Dynam. Astronom.*, 117(2):113–136, 2013.

[47] K. E. Papadakis. Families of three-dimensional periodic solutions in the circular restricted four-body problem. *Astrophys. Space Sci.*, 361(4):Paper No. 129, 14, 2016.

[48] Jaime Burgos-Garcí a. Families of periodic orbits in the planar Hill's four-body problem. *Astrophys. Space Sci.*, 361(11):Paper No. 353, 21, 2016.

[49] K. E. Papadakis. Families of asymmetric periodic solutions in the restricted four-body problem. *Astrophys. Space Sci.*, 361(12):Paper No. 377, 15, 2016.

[50] D. Blazevski and C. Ocampo. Periodic orbits in the concentric circular restricted four-body problem and their invariant manifolds. *Phys. D*, 241(13):1158–1167, 2012.

[51] Maxime Murry and J. D. Mireles James. Chebyshev-taylor parameterization of stable/unstable manifolds for periodic orbits: implementation and applications. *(Submitted)*, pages 1–32, 2017.

[52] M. Alvarez-Ramí rez and E. Barrabés. Transport orbits in an equilateral restricted four-body problem. *Celestial Mech. Dynam. Astronom.*, 121(2):191–210, 2015.

[53] Martha Álvarez-Ramí rez and Claudio Vidal. Dynamical aspects of an equilateral restricted four-body problem. *Math. Probl. Eng.*, pages Art. ID 181360, 23, 2009.

[54] Marian Gidea and Melissa Burgos. Chaotic transfers in three- and four-body systems. *Phys. A*, 328(3-4):360–366, 2003.

[55] Zhikun She, Xuhua Cheng, and Cuiping Li. The existence of transversal homoclinic orbits in a planar circular restricted four-body problem. *Celestial Mech. Dynam. Astronom.*, 115(3):299–309, 2013.

[56] Zhikun She and Xuhua Cheng. The existence of a Smale horseshoe in a planar circular restricted four-body problem. *Celestial Mech. Dynam. Astronom.*, 118(2):115–127, 2014.

[57] Xuhua Cheng and Zhikun She. Study on chaotic behavior of the restricted four-body problem with an equilateral triangle configuration. *Internat. J. Bifur. Chaos Appl. Sci. Engrg.*, 27(2):1750026, 12, 2017.

[58] Martha Alvarez-Ramí rez, Joaquí n Delgado, and Claudio Vidal. Global regularization of a restricted four-body problem. *Internat. J. Bifur. Chaos Appl. Sci. Engrg.*, 24(7):1450092, 15, 2014.

[59] Jaime Burgos-Garcí a and Marian Gidea. Hill's approximation in a restricted four-body problem. *Celestial Mech. Dynam. Astronom.*, 122(2):117–141, 2015.

[60] John M. Lee. *Introduction to smooth manifolds*, volume 218 of *Graduate Texts in Mathematics*. Springer, New York, second edition, 2013.

[61] Shane Kepley and J. D. Mireles James. Chaotic motions in the restricted four body problem (ii): rigorous error estimates and implementation details. *(In preperation)*, pages 1–55, 2017.

[62] Oscar E. Lanford, III. A computer-assisted proof of the Feigenbaum conjectures. *Bull. Amer. Math. Soc. (N.S.)*, 6(3):427–434, 1982.

[63] Oscar E. Lanford, III. A shorter proof of the existence of the Feigenbaum fixed point. *Comm. Math. Phys.*, 96(4):521–538, 1984.

[64] Jean-Pierre Eckmann and Peter Wittwer. A complete proof of the Feigenbaum conjectures. *J. Statist. Phys.*, 46(3-4):455–475, 1987.

[65] J.-P. Eckmann, H. Koch, and P. Wittwer. A computer-assisted proof of universality for area-preserving maps. *Mem. Amer. Math. Soc.*, 47(289):vi+122, 1984.

[66] Oscar E. Lanford, III. Computer-assisted proofs in analysis. *Phys. A*, 124(1-3):465–470, 1984. Mathematical physics, VII (Boulder, Colo., 1983).

[67] J. B. van den Berg and J.P. Lessard. Rigorous numerics in dynamics. *Notices Amer. Math. Soc.*, 62(9):1057–1061, 2015.

[68] Siegfried M. Rump. Verification methods: rigorous results using floating-point arithmetic. *Acta Numer.*, 19:287–449, 2010.

[69] X. Cabré, E. Fontich, and R. de la Llave. The parameterization method for invariant manifolds. I. Manifolds associated to non-resonant subspaces. *Indiana Univ. Math. J.*, 52(2):283–328, 2003.

[70] X. Cabré, E. Fontich, and R. de la Llave. The parameterization method for invariant manifolds. II. Regularity with respect to parameters. *Indiana Univ. Math. J.*, 52(2):329–360, 2003.

[71] X. Cabré, E. Fontich, and R. de la Llave. The parameterization method for invariant manifolds. III. Overview and applications. *J. Differential Equations*, 218(2):444–515, 2005.

[72] À. Haro and R. de la Llave. A parameterization method for the computation of invariant tori and their whiskers in quasi-periodic maps: numerical algorithms. *Discrete Contin. Dyn. Syst. Ser. B*, 6(6):1261–1300 (electronic), 2006.

[73] A. Haro and R. de la Llave. A parameterization method for the computation of invariant tori and their whiskers in quasi-periodic maps: rigorous results. *J. Differential Equations*, 228(2):530–579, 2006.

[74] A. Haro and R. de la Llave. A parameterization method for the computation of invariant tori and their whiskers in quasi-periodic maps: explorations and mechanisms for the breakdown of hyperbolicity. *SIAM J. Appl. Dyn. Syst.*, 6(1):142–207 (electronic), 2007.

[75] Àlex Haro, Marta Canadell, Jordi-Lluí s Figueras, Alejandro Luque, and Josep-Maria Mondelo. *The parameterization method for invariant manifolds*, volume 195 of *Applied Mathematical Sciences*. Springer, [Cham], 2016. From rigorous results to effective computations.

[76] J. B. Van den Berg, J. D. Mireles James, and Christian Reinhardt. Computing (un)stable manifolds with validated error bounds: non-resonant and resonant spectra. *Journal of Nonlinear Science*, 26:1055–1095, 2016.

[77] J. D. Mireles James. Validated numerics for equilibriua of analytic vector fields: invariant manifolds and connecting orbits. *(To appear in AMS lecture notes - winter short course series)*, pages 1–55, 2017.

[78] R. de la Llave, A. González, À. Jorba, and J. Villanueva. KAM theory without action-angle variables. *Nonlinearity*, 18(2):855–895, 2005.

[79] J. F. Steffensen. On the differential equations of Hill in the theory of the motion of the moon. *Acta Math.*, 93:169–177, 1955.

[80] Eugene Rabe. Determination and survey of periodic Trojan orbits in the restricted problem of three bodies. *Astronom. J.*, 66:500–513, 1961.

[81] André Drprit and J.F. Price. The computation of characterist exponents in the palnar restricted problem of three bodies. *Boeing Scientific Research Labortories, Mathematics Research Laboratory*, Mathematical Note(Number 415):1–84, 1965.

[82] Donald E. Knuth. *The art of computer programming. Vol. 2.* Addison-Wesley Publishing Co., Reading, Mass., second edition, 1981. Seminumerical algorithms, Addison-Wesley Series in Computer Science and Information Processing.

[83] Maxime Murray and J. D. Mireles James. Chebyshev-taylor parameterization of stable/unstable manifolds for periodic orbits: implementation and applications. *Internat. J. Bifur. Chaos Appl.*, 27(14), 2017.

[84] J. B. van den Berg, Maxime Breden, J.P. Lessard, and Maxime Murray. Continuation of homoclinic orbits in the suspension bridge equation: a computer assisted proof. *(Submitted)* `https://arxiv.org/abs/1702.07412`, 2017.